Tetravalent SARS-CoV-2 S1 Subunit Protein Vaccination Elicits Robust Humoral and Cellular Immune Responses in SIV-Infected Rhesus Macaque Controllers

Muhammad S. Khan[a,b,⊥], Eun Kim[a,⊥], Quentin Le Hingrat[c], Adam Kleinman[c], Alessandro Ferrari[d], Jose C Sammartino[d], Elena Percivalle[d], Cuiling Xu[f], Shaohua Huang[a], Thomas W. Kenniston[a], Irene Cassaniti[d], Fausto Baldanti[d,e], Ivona Pandrea[c,f], Andrea Gambotto[a,b,c,g*], Cristian Apetrei[b,c*]

[a]Department of Surgery, University of Pittsburgh School of Medicine, Pittsburgh, Pennsylvania, PA 15213, USA.
[b]Department of Infectious Diseases and Microbiology, University of Pittsburgh School of Public Health, Pittsburgh, PA, USA
[c]Division of Infectious Diseases, Department of Medicine, University of Pittsburgh School of Medicine, Pittsburgh, PA 15213, USA.
[d]Molecular Virology Unit, Microbiology and Virology Department, IRCCS Policlinico San Matteo, Via Taramelli 5, 27100 Pavia, Italy
[e]Department of Clinical, Surgical, Diagnostic and Pediatric Sciences, University of Pavia, 27100 Pavia, Italy
[f]Department of Pathology, University of Pittsburgh School of Medicine, Pittsburgh, PA 15213, USA.
[g]UPMC Hillman Cancer Center, Pittsburgh, PA 15232, USA

[⊥]Authors Contributed Equally

***Corresponding Authors**
Andrea Gambotto, MD
Department of Surgery, University of Pittsburgh School of Medicine
W1148 Biomedical Science Tower
200 Lothrop St. Pittsburgh, PA 15261, USA
Tel.: +1-412-383-6151; Fax: +1-412-624-3365
Email: gambottoa@upmc.edu

Cristian Apetrei, MD, PhD
Division of Infectious Diseases, Department of Medicine, University of Pittsburgh School of Medicine;
3550 Terrace St., Pittsburgh, PA 15261, USA
Tel.: +1-412-383-5256; Fax: +1-412-648-8521
Email: apetreic@pitt.edu

Keywords: COVID-19, vaccine, protein subunit, tetravalent, SARS-CoV-2, nonhuman primate, immunogenicity, efficacy, humoral immunity, cellular immunity.

Abstract

The COVID-19 pandemic has highlighted the need for safe and effective vaccines to be rapidly developed and distributed worldwide, especially considering the emergence of new SARS-CoV-2 variants. Protein subunit vaccines have emerged as a promising approach due to their proven safety record and ability to elicit robust immune responses. In this study, we evaluated the immunogenicity and efficacy of an adjuvanted tetravalent S1 subunit protein COVID-19 vaccine candidate composed of the Wuhan, B.1.1.7 variant, B.1.351 variant, and P.1 variant spike proteins in a nonhuman primate model with controlled SIVsab infection. The vaccine candidate induced both humoral and cellular immune responses, with T- and B cell responses mainly peaking post-boost immunization. The vaccine also elicited neutralizing and cross-reactive antibodies, ACE2 blocking antibodies, and T-cell responses, including spike specific $CD4^+$ T cells. Importantly, the vaccine candidate was able to generate Omicron variant spike binding and ACE2 blocking antibodies without specifically vaccinating with Omicron, suggesting potential broad protection against emerging variants. The tetravalent composition of the vaccine candidate has significant implications for COVID-19 vaccine development and implementation, providing broad antibody responses against numerous SARS-CoV-2 variants.

Introduction

The coronavirus disease 2019 (COVID-19) pandemic caused by the severe acute respiratory syndrome coronavirus 2 (SARS-CoV-2) has had an unprecedented impact on global health, economy, and society. The COVID-19 pandemic consisted of over 675 million cases, with 6.5 million deaths, and 13 billion COVID-19 vaccine doses administered across the human population, as of February 3rd 2023.[1] Although approved COVID-19 vaccines have been effective in reducing mortality and morbidity caused by SARS-CoV-2 infection, the emergence of new variants that are able to evade the immune response has raised concerns about their long-term efficacy. Furthermore, the uneven distribution of vaccines worldwide has resulted in many low to middle income countries being left without access to variant-specific vaccines that are better suited for the evolving SARS-CoV-2 variant landscape. This highlights the need for the development of vaccines that can provide broad protection against a range of SARS-CoV-2 variants, as well as the importance of equitable distribution of vaccines to mitigate the risk of further virus evolution and spread.[2–5] Since its emergence in late 2019, SARS-CoV-2 has continuously evolved, at a higher-than-expected rate, giving rise to multiple variants with multiple genetic mutations and various phenotypic properties, including increased transmissibility, virulence, and immune escape.[5,6] The emergence of these variants has raised concerns about the efficacy of current vaccines and the potential for future outbreaks. Therefore, there is a critical need to develop effective vaccines that can provide broad and durable protection against SARS-CoV-2 and its variants. SARS-CoV-2 variants such as B.1.1.7 (Alpha), B.1.351 (Beta), and P.1 (Gamma) have exhibited substantial increases in immune escape from wildtype (WU) vaccine or infection induced immunity.[7,8]

The spike (S) protein of SARS-CoV-2 has been the main target of currently approved COVID-19 vaccines and of most COVID-19 vaccines in development.[9] S protein allows for virus binding and infection of susceptible cells through interaction with host receptor angiotensin-converting enzyme 2 (ACE2).[10] The S1 subunit of the S protein contains the receptor binding domain (RBD) that binds with ACE2, while the S2 subunit allows for cell fusion and viral entry.[11,12] It has been widely acknowledged that antibodies targeting the S protein, particularly those binding to the RBD, are able to block the binding of SARS-CoV-2 to the cell receptor and prevent infection of susceptible cells.[13–17] We have previously demonstrated the immunogenicity of S1 subunit targeting vaccines against various Beta-coronaviruses including SARS-CoV-1, SARS-CoV-2, and MERS.[18–23]

A focus for next-generation SARS-CoV-2 vaccine design is the investigation of novel vaccines which may be able to induce a broader immune response effective against multiple SARS-CoV-2 variants. A multivalent vaccine is a traditional approach used to increase antigen immunity coverage against multi-variant viruses such as SARS-CoV-2. We have previously demonstrated the immunogenicity of a trivalent protein subunit vaccine in BALB/c mice.[22] Here, we assessed our S1 protein subunit vaccine, at an increased valency to tetravalent, in an advanced animal model more closely related to humans. Nonhuman primates (NHPs) are commonly used as preclinical models to evaluate the safety and efficacy of vaccines and therapeutics for infectious diseases, including SARS-CoV-2.[24–27] We employed a rhesus macaque (RM) model of controlled simian immunodeficiency virus (SIV) infection to evaluate the immunogenicity of a tetravalent SARS-CoV-2 S1 protein subunit vaccine delivered with AddaVax adjuvant. Controlled SIV infection in RMs mimic a situation of chronic viral infection which can be encountered in humans, which may influence the development of immune

responses to vaccination. Indeed, some studies reported lower SARS-CoV-2 antibody responses for people living with HIV.[28,29] Several studies have demonstrated the utility of RMs as a preclinical model for SARS-CoV-2 vaccine development. For example, macaques have been used to evaluate the immunogenicity and the correlates of protection, as well as the protective efficacy of various vaccine platforms, including viral vector-based vaccines, mRNA vaccines, and protein subunit vaccines.[26,27,30–34] Moreover, the use of NHP models can provide critical insights into the mechanisms of vaccine-induced immunity, including the kinetics, specificity, and durability of the immune responses.

Here, we evaluated the immunogenicity of a tetravalent SARS-CoV-2 vaccine approach with S1 subunit protein vaccine targeting Wuhan S1, B.1.1.7 (Alpha), B.1.351 (Beta), and P.1 (Gamma). We chose these variants because, at the time of the start of the study, they represented a diverse and relevant set of SARS-CoV-2 strains that were circulating in different regions of the world and had distinct mutations in the spike protein, which is the main target of neutralizing antibodies. We found that vaccination induced robust humoral and cellular immune responses which resulted in antibodies capable of blocking ACE2 binding to 15 different SARS-CoV-2 variants, including multiple Omicron variants. Vaccination also induced antibodies that were able to block SARS-CoV-2 infection of susceptible cells by live wild-type (WU), Beta, and Delta variant viruses. We profiled the lymphocyte response to immunization for 2 months post initial prime vaccination through quantifying the number of T and B cells, investigating markers of T-cell activation, and memory subsets in peripheral blood mononuclear cells (PBMCs) and showed robust immune activation, primarily after boost immunization. We were also able to measure a spike-specific $CD4^+$ T-cell response in the PBMC's of RMs 42 days post-prime immunization, although, no $CD8^+$ T-cell response was found. Our study further demonstrates the

immunogenicity of protein subunit vaccines against SARS-CoV-2 targeting the S1 subunit of the spike protein while also contributing insights on approaches to further increase valency of currently approved COVID-19 vaccines.

Results

Design and expression or recombinant proteins

To produce recombinant proteins of SARS-CoV-2-S1 pAd/S1Wu, pAd/S1Alpha, pAd/S1Beta, and pAd/S1Gamma were generated by subcloning the codon-optimized SARS-CoV-2-S1 gene having C-tag into the shuttle vector, pAd (GenBank U62024) at *Sal* I and *Not* I sites (**Fig. 1A**). Variant-specific mutations for B.1.1.7 (Alpha), B.1.351 (Beta), and P.1 (Gamma) SARS-CoV-2 recombinant S1 proteins are outlined. To determine SARS-CoV-2-S1 expression from each plasmid, Expi293 cells were transfected with pAd/ S1WU, pAd/S1Alpha, pAd/S1Beta, and pAd/S1Gamma or pAd as a control. At 5 days after transfection, the supernatants of Expi293 cells were characterized by Western blot analysis. As shown in **Fig. 1B**, each S1 recombinant proteins were recognized by a polyclonal anti-spike of SARS-CoV-2 Wuhan antibody at the expected glycosylated monomeric molecular weights of about 110 kDa under the denaturing reduced conditions, while no expression was detected in the mock-transfected cells (lane1). The purified rS1WU, rS1Apha, rS1Beta, and rS1Gamma proteins using C-tagXL affinity matrix were determined by silver staining (**Fig. 1C**).

Binding antibody and cross-variant live virus neutralizing antibody response

Prior to immunization, RMs were infected with a simian immunodeficiency virus (SIV) that naturally infects African green monkeys (SIVsab).[35] This virus is completely controlled in

RMs,[36] in spite of retaining the replicative abilities.[37] At the time of SARS-CoV-2 immunization, the RMs were controlling SIVsab for over a year. Upon prime and boost immunization, SIVsab viral loads remained undetectable suggesting no SIV activation upon vaccination. RMs were primed and boosted on week 3 with 60 µg total of rS1WU, rS1Apha, rS1Beta, and rS1Gamma, 15 µg of each antigen, mixed with 300 µl of AddaVax^{TM}, squalene-based oil in water nano-emulsion adjuvant (**Fig. 2A**). To assess the magnitude of the antibody response we first determined Wuhan IgG antibody endpoint titers (EPT) in the sera of vaccinated RMs with ELISA. Serum samples collected prior to immunization, week 3, week 7, and week 9-11 after immunization were serially diluted to determine SARS-CoV-2-S1-specific IgG titers against Wuhan S1 using ELISA (**Fig. 2B**). RMs had detectable anti-S1 binding antibody response prior to immunization (**Fig 2B**), however, no neutralizing antibody response was found (**Fig. 2C**). S1-specific IgG titers were statistically increased at week 7 and week 9-11 when compared to week 0 (**Fig. 2B,** $p < 0.05$, Kruskal-Wallis test, followed by Dunn's multiple comparisons). To evaluate the functional quality of vaccine-generate antigen-specific antibodies, we used a microneutralization assay (NT_{90}) to test the ability of sera from immunized RMs to neutralize the infectivity of SARS-CoV-2. Sera, collected from RMs on week 3 (prior to booster immunization) and week 7 (4 weeks post boost) after primary immunization were tested for the presence of SARS-CoV-2-specific neutralizing antibodies with live SARS-CoV-2 Wuhan, Beta, and Delta viruses (**Fig. 2C**). High levels of neutralizing antibodies were detected in sera at week 3 and week 7 against Wuhan, Beta, and Delta SARS-CoV-2 variants (**Fig. 2C**) and showed a similar pattern with IgG endpoint titers in each RM (**Supplementary Fig. 2**). Furthermore, the geometric mean titers (GMT) of neutralizing antibodies at week 7 against the Wuhan, Beta, and Delta strain were increased with 6.4-, 5.4-, 3.2-fold compared at week 3, respectively, while

only neutralizing antibody response against live Wuhan SARS-CoV-2 at week 7 was significantly increased when compared to preimmunized sera (**Fig. 2C**, $p < 0.05$, Kruskal-Wallis test, followed by Dunn's multiple comparisons). Neutralization against highly immune-evasive Beta and Delta SARS-CoV-2 variants of concern (VOC) were found at slightly lower levels than Wuhan at both week 3 and week 7 (**Fig. 2C**). While Beta VOC S1 was included in the tetravalent immunization regimen, Delta VOC was not, highlighting the diverse response induced by tetravalent immunization in RMs.

Potent ACE2 binding inhibition effective against 15 different SARS-COV-2 VOC's spikes

For further insight into the neutralizing capabilities of antibodies induced by vaccination we used the Meso Scale Discovery (MSD) V-PLEX SARS-CoV-2 (ACE2) Kit to measure the inhibition of binding between angiotensin converting enzyme-2 (ACE2) and trimeric spike protein of SARS CoV-2 variants. Initially, we used kit Panel 18 including Wuhan S and spikes from variants; Alpha (B.1.1.7), Beta (B.1.351), Gamma (P.1), Delta (B.1.617, B.1.617.2), Zeta (P.2), Kappa (B.1.617.1), B.1.526.1, B.1.617, and B.1.617.3 (**Fig. 3**). Sera from vaccinated RMs were examined at week 7, due to that being the peak of measured IgG binding antibody response and compared to preimmunized sera (**Fig. 2A, Fig. 3**). Antibodies blocking ACE2 and trimeric S binding of all variants, by over 90% inhibition, were detected in all 1:10 diluted RM sera at Week 7 (**Fig. 3**). Week 7 sera ACE2 binding inhibition for RMs was significantly increased, when compared to preimmunized sera, for Wuhan, B.1.1.7, B.1.351, P.1, B.1.617.2, P.2, B.1.617.1, B.1.526.1, B.1.617, and B.1.617.3 Spike (**Fig. 3**, $p < 0.05$, Mann-Whitney Test).

To assess the neutralizing capabilities of RM vaccine induced antibodies against Omicron (BA.1) VOC, and Omicron sub-variants (BA.2, BA.3, BA.1+R346K, BA.1+L452R) we used MSD V-Plex SARS-CoV-2 ACE2 Kit Panel 25 (**Fig. 4**). Panel 25 includes SARS-CoV-2 Wuhan, BA.1, BA.2, AY.4, BA.3, BA.1+R346K, BA.1+L452, B.1.1.7, B.1.351, and B.1.640.2 trimeric spike. Sera from vaccinated RMs were examined at week 3, week 7, and week 9-11 post vaccination and compared to preimmunized sera at a 1:10 dilution (**Fig. 4A**) and 1:100 dilution (**Fig 4B**). Week 7 and Week 9-11 RM sera ACE2-binding inhibition were significantly increased when compared to preimmunized sera for Wuhan, AY.4 (Delta lineage), BA.1+L452R, B.1.1.7, B.1.351, and B.1.640.2 VOC spikes at 1:10 dilution (**Fig. 4A**, $p < 0.05$, Kruskal-Wallis test, followed by Dunn's multiple comparisons). Week 7 RM sera ACE2-binding inhibition were significantly increased when compared to preimmunized sera for BA.1 VOC spike at 1:10 dilution (**Fig. 4A** $p < 0.05$, Kruskal-Wallis test, followed by Dunn's multiple comparisons).While not statistically significantly increased when compared to preimmunized RM sera; RMs demonstrated moderate ACE2-binding inhibition for BA.2, BA.3, and BA.1+R346K VOC spikes weeks 7 and 9-11 post immunization at 1:10 dilution (**Fig. 4A**, $p > 0.05$, Kruskal-Wallis test, followed by Dunn's multiple comparisons). To further interrogate the vaccine-induced neutralizing capabilities of RMs, we further substantially diluted RM sera to 1:100 (**Fig. 4B**). Week 7 RM 1:100 diluted sera ACE-2 binding inhibition was significantly increased when compared to preimmunized sera for Wuhan, AY.4, B.1.1.7, B.1.351, B.1.640.2 VOC spikes (**Fig. 4B**, $p < 0.05$, Kruskal-Wallis test, followed by Dunn's multiple comparisons). At 1:100 dilution, RM sera did not have ACE-2 binding inhibition above preimmunized sera for BA.1, BA.2, BA.3, BA.1+R346K, BA.1+L452R VOC spikes (**Fig. 4B**). Results suggest the necessity of the booster immunization to induce potent and cross variant recognizing antibodies.

Results also suggest that vaccination induced antibodies that are able to potently recognize and block ACE2 binding of a wide range of SARS-CoV-2 variants spikes by week 7 post prime immunization.

Longitudinal lymphocyte dynamics and cell-mediate immune response to vaccination shows immune activation primarily observed after boost

To investigate the kinetics and magnitude of immune responses induced by the tetravalent SARS-CoV-2 vaccine, we monitored the peripheral blood mononuclear cells (PBMCs) of vaccinated rhesus macaques over a 60-day period. PBMCs are a mixture of different immune cell types, including T cells and B cells, and are a useful tool for investigating the immune response to vaccination in vivo.

Fig. 5 shows the dynamics of $CD3^+$ T-cells (**Fig. 5A**), $CD4^+$ T-cells (**Fig. 5B**), $CD8^+$ T-cells (**Fig. 5C**), and $CD20^+$ B cell (**Fig. 5D**) counts over 60 days. We observed increases in all T-cell subsets ($CD3^+$, $CD4^+$, and $CD8^+$) and B cells ($CD20^+$) after the prime and especially after the boost, demonstrating clear increases for all subsets, with the $CD8^+$ T cell count showing the greatest increase after boost immunization compared to the other cell types.

Fig. 6 shows the fraction of activating and proliferating $CD4^+$ and $CD8^+$ T cells. We used the activation markers CD69 and HLDR and CD38, as previously described in the literature.[38–40] We also used Ki-67 as a marker for cell proliferation. $CD69^+$ $CD4^+$ T-cell induction was mainly observed in RM177 (**Fig. 6A**). $Ki67^+$ $CD4^+$ T cells showed moderate increases in percentage after boost vaccination (**Fig. 6B**). HLA-DR^+ $CD38^+$ $CD4^+$ T-cells showed activation post prime and boost with a return to near baseline by Day 40 (**Fig. 6C**). The fraction of $CD69^+$ $CD8^+$ T-cells increased in all RMs post prime and boost, with most starting to return to prevaccination

levels at day 60 (**Fig. 6D**). The induction of Ki-67$^+$ CD8$^+$ T-cells was primarily seen at day 40 postimmunization (**Fig. 6E**), while HLA-DR$^+$ CD38$^+$ CD8$^+$ T-cell activation was mainly seen in RM175 and RM176 at different timepoints (**Fig. 6F**). However, the induction of HLA-DR$^+$ CD38$^+$ CD8$^+$ T cells was not as robust as that of CD69$^+$ CD8$^+$ T cells and Ki-67$^+$ CD8$^+$ T cells (**Fig. 6F, Fig. 6D, Fig. 6E**).

Fig. 7 shows the changes in the distribution of T-cell memory subsets over time. We defined naïve, central memory (CM), and effector memory (EM) T cells using CD28$^+$ and CD95$^+$ markers. Naïve T cells are CD28$^+$ CD95^{neg}, CM T-cells are CD28$^+$ CD95$^+$, and EM T cells are CD28^{neg} CD95$^+$. We observed that both CD4$^+$ and CD8$^+$ central memory T cells (**Fig. 7A & 7D**), along with naïve CD4$^+$ naïve CD8$^+$ T cells (**Fig. 7C & 7F**), decreased in abundance after prime and boost, while CD4$^+$ and CD8$^+$ effector memory T cells (**Fig. 7B & 7E**) increased in abundance after prime boost. This finding suggests that the tetravalent S1 protein vaccine induces a shift towards an effector memory phenotype and away from a central memory phenotype, which may be beneficial in generating a rapid and robust response to vaccination.

Intracellular cytokine staining was performed to evaluate the spike-specific T-cell responses in CD4$^+$ and CD8$^+$ T cells after stimulation with a spike peptide pool at day 0 and day 42 postvaccination in PBMCs (**Fig. 8**). We tested for interferon-gamma (IFN-γ), interleukin-2 (IL-2), and tumor necrosis factor-alpha (TNF-α) cytokine staining. Only RM212 induced an IFN-γ CD4$^+$ T-cell response, while no such response was observed in the other four RMs (**Fig. 8A**). In **Fig. 8B**, we observed an induction of IL-2 CD4$^+$ T-cell response in RM212 and to a lesser extent in RM101, but not in the other three RMs. **Fig. 8C** shows an induction of TNFα CD4$^+$ T-cell response in RM212, RM176 and, to a minimal extent, in RM101, RM175, and RM177. Notably, we were not able to detect a spike specific CD8$^+$ T-cell response at day 0 or day 42 post

vaccination (data not shown). RM212 mounted a robust $CD4^+$ T-cell response for all three cytokines at day 42. These results suggest that there is a variable induction of cytokine responses in $CD4^+$ T cells among different RMs at day 42 postvaccination.

Overall, the use of PBMC's allowed for the unique assessment of the dynamics of immune activation after vaccination. The results showed a clear increase in T-cell counts and activation after boost immunization, with the $CD8^+$ T-cell counts showing the greatest increase. The use of CD markers allowed for the differentiation of T-cell subsets and their activation status, with the $CD8^+$ T cells expressing either CD69 or Ki-67 $CD8^+$ T cells showing the most robust dynamics. Additionally, there was evidence of a functional spike-specific $CD4^+$ T-cell response in RMs at day 42 post vaccination, albeit in the context of no $CD8^+$ T-cell response. These findings highlight the potential of this vaccine candidate to induce a robust cellular immune response, which is critical for controlling viral infections.

Discussion

We evaluated the immunogenicity and efficacy of a tetravalent COVID-19 vaccine candidate based on the spike S1 protein of SARS-CoV-2 in an NHP model of controlled SIV infection. RMs infected with SIVsab from African green monkeys are able to control viral replication and disease progression through maintaining a healthy immune system, unlike HIV-1 in humans.[36] The SIVsab-infected RMs in this study were elite controllers for about a year prior to SARS-CoV-2 immunization.

There were weaker band in western blot of the supernatant after a transient transfection with pAd/S1Alpha, pAd/S1Beta, and pAd/S1Gamma compared with pAd/S1WU **(Fig. 1B)**, which might be explained by the usage of anti-spike of SARS-CoV-2 Wuhan as a primary

antibody**.** Indeed, no big differences were observed in yield pre or post C-tag purification of each recombinant proteins after transient transfection by sandwich ELISA with standard of each purified rS1 proteins **(Supplementary Fig.1).**

Our vaccine formulation induced high levels of binding antibodies against the Wuhan strain of SARS-CoV-2, as well as neutralizing antibodies against live B.1.351 (Beta), and B.1.617.2 (Delta) VOC (**Fig. 2**). The sera of vaccinated RMs exhibited potent ACE2-binding inhibition capabilities against a suite of SARS-CoV-2 VOC spikes including Omicron (BA.1) and Omicron subvariants (BA.2, BA.3, BA.1+R246K, and BA.1+L452R) (**Fig. 3 & Fig. 4**). These findings are consistent with previous studies demonstrating the immunogenicity and cross-reactivity of COVID-19 vaccines NHP models.[26,27,30–33,41]

Importantly, the vaccine candidate also induced cellular immune responses, including T cell responses, which have been shown to play a critical role in COVID-19 immunity and protection.[42–49] We investigated the cellular immune response to the tetravalent SARS-CoV-2 vaccine in vaccinated RMs, using a range of markers to examine T-cell subsets and activation status. The results showed that all T-cell subsets and B cells increased after the prime and especially after the boost, with the $CD8^+$ T-cell count showing the greatest increase after boost immunization compared to other cell types (**Fig. 5**). We demonstrate that the tetravalent S1 subunit protein COVID-19 vaccine candidate induces $CD4^+$ and $CD8^+$ T-cell activation, as indicated by increased expression of CD69, HLA-DR, CD38, and Ki-67 activation and proliferation markers on both T-cell subsets (**Fig. 6**). The distribution of T-cell memory subsets over time was also investigated, revealing a decrease in abundance of both $CD4^+$ and $CD8^+$ central memory T cells, along with $CD4^+$ and $CD8^+$ naive T cells after prime and boost (**Fig. 7**). In contrast, $CD4^+$ and $CD8^+$ effector memory T cells increased in abundance after prime boost,

indicating a shift towards an effector memory phenotype and away from a central memory phenotype induced by the tetravalent S1 protein vaccine (**Fig. 7**). Furthermore, intracellular cytokine staining was performed to evaluate the spike-specific responses of $CD4^+$ and $CD8^+$ T cells after stimulation with a spike peptide pool (**Fig. 8**). Cytokine staining for IFN-γ, IL-2, and TNF-α was tested and a variable induction of cytokine responses by $CD4^+$ T cells among different RMs at day 42 postvaccination was observed (**Fig. 8**). However, no spike-specific response of the $CD8^+$ T cells was detected at day 0 or day 42. It is possible that the spike-specific $CD8^+$ T cells were present, but were not detected by the intracellular staining assay, as this assay may not be sensitive enough to detect low-frequency antigen-specific $CD8^+$ T cells. It is also possible that the undetectable spike-specific $CD8^+$ T-cell response at day 42 post-vaccination was related to the time-point used, which was too late after boost, such as the vaccine-specific T cells had already started to wane in abundance, as shown by Arunachalam et al.[50] Altogether, our study demonstrates that the tetravalent S1 protein vaccine candidate was able to induce a robust SARS-CoV-2-specific immune response in RMs, which is promising for future development and testing of COVID-19 vaccines in humans.

The results of our study have important implications for COVID-19 vaccine development and implementation in humans. The vaccine candidate induced not only humoral immune responses but also cellular immune responses, which have been shown to be important for long-term immunity.[51] The use of RMs as an animal model for studying vaccine efficacy has been widely accepted in the scientific community.[25,26,34,52] Here we have used RM controllers based on the rationale that SIV controllers have a nearly healthy immune system (able to control SIV replication).[36] We also wanted to assess whether the induction of T-cell activation at the effector sites would result in a burst of SIV replication. Such a boosting of SIV was reported to occur

after administration of vectorized vaccines.[53] The use of NHP models has been shown to be highly informative for predicting vaccine efficacy in humans.[54,55]

The results showed that the vaccine induced both humoral and cellular immune responses against SARS-CoV-2, including neutralizing antibodies, ACE2 blocking antibodies, and T-cell responses. Furthermore, the vaccine candidate was able to generate Omicron variant binding and ACE2 blocking antibodies without specifically vaccinating with Omicron, suggesting the potential for broad protection against emerging variants.[56–60] This is particularly significant given the emergence of highly diverged SARS-CoV-2 variants, such as Omicron, which have raised concerns about vaccine efficacy and the need for updated vaccines.[56,58,59,61] Another significant feature of the vaccine candidate is its tetravalent composition, which targets the spike proteins of four different SARS-CoV-2 variants. This approach has the potential to provide broad protection against multiple SARS-CoV-2 variants, as well as to minimize the risk of immune escape and emergence of new variants.

Protein subunit vaccines are known for their safety, ease of large-scale production, and distribution, and have been used in other successful vaccine campaigns, such as the hepatitis B vaccine.[54,62–64] This makes protein subunit vaccines an ideal candidate for worldwide vaccine equity, particularly for countries that may not have access to the more complex mRNA or viral vector vaccine platforms. Furthermore, the ability to store and transport protein subunit vaccines at a relatively low temperature (-20°C to 4°C) , compared to the ultra-low temperature required for mRNA vaccines, makes their distribution and administration easier in resource-limited settings.[65,66] The protein subunit platform is also amenable to alternative routes of administration, such as intradermal delivery, which has been shown to increase immunogenicity in other vaccine studies.[20,67–69] In summary, the tetravalent S1 protein subunit vaccine represents a promising

vaccine candidate against SARS-CoV-2, particularly for populations that may not have access to other vaccine platforms and could potentially be further optimized to enhance its immunogenicity.

However, it should be noted that this study has limitations. The sample size was small and we did not perform a SARS-CoV-2 virus challenge in our vaccinated RMs to fully assess vaccine efficacy.[27,50] While our results show promising immune responses to the tetravalent SARS-CoV-2 vaccine in RMs, a virus challenge would have provided further insights into the effectiveness of the vaccine in preventing infection and disease. Additionally, our study did not evaluate the durability of the antibody response generated by the vaccine over a longer period. Studies have shown that antibody responses to SARS-CoV-2 vaccines may wane over time, which highlights the importance of evaluating the longevity of vaccine-induced immunity.[70–75] Finally, we did not assess mucosal immunity in our study, which is an important aspect of immune protection against respiratory viruses like SARS-CoV-2. Mucosal immunity may provide an additional layer of protection against infection and transmission, and future studies should investigate the mucosal immune response to the tetravalent SARS-CoV-2 vaccine.[31,76–79]

The tetravalent S1 subunit protein COVID-19 vaccine candidate evaluated in this study contained SARS-CoV-2 S1 antigens from the Wuhan strain, as well as the B.1.1.7 variant, B.1.351 variant, and P.1 variant. Our study demonstrates that this vaccine candidate can induce both humoral and cellular immune responses, as evidenced by increased cell counts in both T and B cells, and the production of neutralizing and cross-reactive antibodies, as well as ACE2 blocking antibodies and T cell responses. It is important to note that the RMs used in this study were infected with SIVsab and controlled the infection for a year prior to immunization. The ability of these animals to control the SIVsab infection, without reactivation of virus upon

383 immunization, while mounting immune responses to the vaccine candidate, further demonstrates
384 the potential of this vaccine candidate to provide robust protection against SARS-CoV-2, even in
385 individuals with pre-existing conditions. Moreover, the tetravalent composition of the vaccine
386 candidate has significant implications for COVID-19 vaccine development and implementation,
387 with the potential to provide broad protection against multiple SARS-CoV-2 variants and to
388 minimize the risk of immune escape and emergence of new variants.
389

390 # Materials and methods

391 ### Construction of recombinant protein expressing vectors

392 The coding sequence for SARS-CoV-2-S1 amino acids 1 to 661 of full-length from
393 BetaCoV/Wuhan/IPBCAMS-WH-05/2020 (GISAID accession id. EPI_ISL_ 403928) having C-
394 terminal tag known as 'C-tag', composed of the four amino acids (aa), glutamic acid-proline-
395 glutamic acid-alanine (E-P-E-A) flanked with *Sal* I & *Not* I was codon-optimized using the
396 UpGene algorithm for optimal expression in mammalian cells (68) and synthesized (GenScript).
397 The construct also contained a Kozak sequence (GCCACC) at the 5′ end. For Alpha variant
398 (B.1.1.7), SARS-CoV-2-S1 mutated Del69-70; Del144; N501Y; A570D; D614G was
399 synthesized. Also, Beta variant (B.1.351) of SARS-CoV-2-S1 (Del144; K417N; E484K; N501Y;
400 A570D; D614G) and Gamma variant (P.1) of SARS-CoV-2-S1 (L18F; T20N; P26S; D138Y;
401 R190S; K417T; E484K; N501Y; H655Y) were synthesized based on above codon-optimized
402 SARS-CoV-2-S1 Wuhan. pAd/S1WU, pAd/S1Alpha, pAd/S1Beta, and pAd/S1Gamma, were
403 then created by subcloning the four variants of codon-optimized SARS-CoV-2-S1 inserts into the
404 shuttle vector, pAdlox (GenBank U62024), at *Sal* I/*Not* I sites. The plasmid constructs were
405 confirmed by DNA sequencing.

406

407 **Transient Production in Expi293 Cells**

408 pAd/S1WU, pAd/S1Alpha, pAd/S1Beta, and pAd/S1Gamma, were amplified, and
409 purified using ZymoPURE II plasmid maxiprep kit (Zymo Research). For Expi293 cell
410 transfection, we used ExpiFectamie^{TM} 293 Transfection Kit (ThermoFisher) and followed the
411 manufacturer's instructions. Cells were seeded 3.0×10^6 cells/ml one day before transfection and
412 grown to $4.5\text{-}5.5 \times 10^6$ cells/ml. 1μg of DNA and ExpiFectamine mixtures per 1ml culture were
413 combined and incubated for 15 min before adding into 3.0×10^6 cells/ml culture. At 20 h post-
414 transfection, enhancer mixture was added, and culture was shifted to 32°C. The supernatants
415 were harvested 5 days post transfection and clarified by centrifugation to remove cells, filtration
416 through 0.8 μm, 0.45 μm, and 0.22 μm filters and either subjected to further purification or
417 stored at 4°C before purification.

418

419 **SDS-PAGE and western blot**

420 To evaluate the expression of S1 from the plasmids, Expi293 cells were transfected with
421 pAd/S1WU, pAd/S1Alpha, pAd/S1Beta, and pAd/S1Gamma, respectively. At 5 days after
422 transfection, 10 μl each supernatant of Expi293 cells was subjected to sodium dodecyl sulfate
423 polyacrylamide gel electrophoresis (SDS-PAGE) and Western blot as previously described.[20]
424 Briefly, after the supernatants were boiled in Laemmli sample buffer containing 2% SDS with
425 beta-mercaptoethanol (β-ME), the proteins were separated by Tris-Glycine SDS-PAGE gels and
426 transferred to nitrocellulose membrane. After blocking for 1 hour at room temperature (RT) with
427 5% non-fat milk in PBST, rabbit anti-SARS-CoV Wuhan spike polyclonal antibody (1:3000)
428 (Sino Biological) was added and incubated overnight at 4 °C as primary antibody, and

horseradish peroxidase (HRP)-conjugated goat anti-rabbit IgG (1:10000) (Jackson immunoresearch) was added and incubated at RT for 2 hours as secondary antibody. After washing three times with PBST, the signals were visualized on an iBright FL 1500 Imager (ThermoFisher).

Purification of recombinant proteins

The recombinant proteins named rS1WU, rS1Alpha, rS1Beta, and rS1Gamma were purified using a CaptureSelect^{TM} C-tagXL Affinity Matrix prepacked column (ThermoFisher) and followed the manufacturer's guidelines. Briefly, The C-tagXL column was conditioned with 10 column volumes (CV) of equilibrate/wash buffer (20 mM Tris, pH 7.4) before sample application. Supernatant was adjusted to 20 mM Tris with 200 mM Tris (pH 7.4) before being loaded onto a 5-mL prepacked column per the manufacturer's instructions at 5 ml/min rate. The column was then washed by alternating with 10 CV of equilibrate/wash buffer, 10 CV of strong wash buffer (20 mM Tris, 1 M NaCl, 0.05% Tween-20, pH 7.4), and 5 CV of equilibrate/wash buffer. The recombinant proteins were eluted from the column by using elution buffer (20 mM Tris, 2 M $MgCl_2$, pH 7.4). The eluted solution was concentrated and desalted with preservative buffer (PBS) in an Amicon Ultra centrifugal filter devices with a 50,000 molecular weight cutoff (Millipore). The concentrations of the purified recombinant proteins were determined by the BCA protein assay kit (ThermoFisher) and separated by reducing SDS-PAGE and visualized by silver staining. The rest proteins were aliquoted and stored at −80°C until use.

ELISA

Sera from all rhesus macaques were collected prior to immunization and on weeks 3 and 7 after immunization. Sera was evaluated for SARS-CoV-2 S1-specific IgG using ELISA. ELISA plates were coated with 200 ng of recombinant SARS-CoV-2-S1 protein (Sino Biological) per well overnight at 4°C in carbonate coating buffer (pH 9.5) and then blocked with PBS-T and 2% bovine serum albumin (BSA) for one hour. Rhesus macaque sera was inactivated at 64°C for 40 minutes, then diluted in PBS-T with 1% BSA and incubated overnight. After the plates were washing, anti-monkey IgG-horseradish peroxidase (HRP) (1:50000, Sigma) were added to each well and incubated for one hour. The plates were washed three times, developed with 3,3'5,5'-tetramethylbenzidine, and the reaction was stopped with 1M H_2SO_4. Next, absorbance was determined at 450nm using a plate reader (Molecular Devices SPECTRAmax).

Animals and Immunization

At week 0, male RMs (n=5 animals per group) were bled and primed with 60 µg of tetravalent rS1 proteins of Wuhan, B.1.1.7 (Alpha), B.1.351 (Beta), and P.1 (Gamma) [15µg of each antigen]. Total volume of 300 µl of antigen was mixed with 300 µl of AddaVax adjuvant then administered to RMs (600 µl injection volume). RMs were bled on week 3 and received a homologous booster of 60 µg of tetravalent rS1 proteins. RMs were bled on weeks 7. RMs were also bled and serially euthanized after week 9 post-prime vaccination: on day 0 (RM177), 1 (RM175), 6 (RM176), 8 (RM101), and 15 (RM175). PMBC's from RMs were collected and analyzed on Days -1, 3, 7, 10, 14, 21, 24, 28, 31, 35, 42, 49, and 64 days post prime immunization. RMs were maintained under specific pathogen-free conditions at the University of Pittsburgh, and all experiments were conducted in accordance with animal use guidelines and

protocols approved by the University of Pittsburgh's Institutional Animal Care and Use (IACUC) Committee.

SARS-CoV-2 microneutralization assay

Neutralizing antibody (NT-Ab) titers against SARS-CoV-2 were defined according to the following protocol.[80,81] Briefly, 50 µl of sample from each mouse, starting from 1:10 in a twofold dilution, were added in two wells of a flat bottom tissue culture microtiter plate (COSTAR, Corning Incorporated, NY 14831, USA), mixed with an equal volume of 100 TCID50 of a SARS-CoV-2 Wuhan, Beta, or Delta strain isolated from symptomatic patients, previously titrated, and incubated at 33°C in 5% CO_2. All dilutions were made in EMEM (Eagle's Minimum Essential Medium) with addition of 1% penicillin, streptomycin and glutamine and 5 γ/mL of trypsin. After 1 hour incubation at 33°C 5% CO_2, 3×10^4 VERO E6 cells [VERO C1008 (Vero 76, clone E6, Vero E6); ATCC® CRL-1586™] were added to each well. After 72 hours of incubation at 33°C 5% CO_2 wells were stained with Gram's crystal violet solution (Merck KGaA, 64271 Damstadt, Germany) plus 5% formaldehyde 40% m/v (Carlo ErbaSpA, Arese (MI), Italy) for 30 min. Microtiter plates were then washed in running water. Wells were scored to evaluate the degree of cytopathic effect (CPE) compared to the virus control. Blue staining of wells indicated the presence of neutralizing antibodies. Neutralizing titer was the maximum dilution with the reduction of 90% of CPE. A positive titer was equal or greater than 1:10. The geometric mean titers (GMT) of NT_{90} end point titer were calculated with 4 as a negative shown <10. Sera from mice before vaccine administration were always included in microneutralizaiton (NT) assay as a negative control.

496 **ACE2 Blocking Assay**

497 Antibodies blocking the binding of SARS-CoV-2 spike variants (Alpha (B.1.1.7), Beta
498 (B.1.351), Gamma (P.1), Delta (B.1.617.2), Zeta (P.2), Kappa (B.1.617.1), New York
499 (B.1.516.1), India (B.1.617 and B.1.617.3)) to ACE2 were detected with a V-PLEX SARS-CoV-
500 2 Panel 18 (ACE2) Kit (Meso Scale Discovery (MSD) according to the manufacturer's
501 instructions. Antibodies blocking the binding of SARS-CoV-2 spike including Wuhan and spikes
502 from immune evasive variants; BA.1, BA.2, AY.4 (Delta lineage), BA.3, BA.1+R346K
503 mutation, BA.1+L452R mutation, B.1.1.7 (Alpha), B.1.351 (Beta), and B.1.1640.2 to ACE2
504 were detected with a V-PLEX SARS-CoV-2 Panel 25 (ACE2) Kit (Meso Scale Discovery
505 (MSD) according to the manufacturer's instructions. Serum samples were diluted (1:10 and
506 1:100). The assay plate was blocked for 30 min and washed. Serum samples were diluted (1:10
507 for P18; 1:10 & 1:100 for P25) and 25 µl were transferred to each well. The plate was then
508 incubated at room temperature for 60 min with shaking at 700 rpm, followed by the addition of
509 SULFO-TAG conjugated ACE2, and continued incubation with shaking for 60 min. The plate
510 was washed, 150 µl MSD GOLD Read Buffer B was added to each well, and the plate was read
511 using the QuickPlex SQ 120 Imager. Electrochemiluminescent values (ECL) were generated for
512 each sample. Results were calculated as % inhibition compared to the negative control for the
513 ACE2 inhibition assay, and % inhibition is calculated as follows: % neutralization = 100 × (1 −
514 (sample signal/negative control signal).
515

516 **Flow Cytometry**

517 Absolute counts of immune cells in whole blood and immunophenotyping of circulating
518 immune cells were determined by flow cytometry. First, 50 µl of whole blood were added to a

519 TruCount tube (BD Biosciences) containing an antibody mix, allowing to precisely quantify
520 $CD45^+$ cell counts in blood, as well as $CD4^+$ and $CD8^+$ T cells, and $CD20^+$ B cells. Whole
521 peripheral blood was stained with fluorescently-labeled antibodies (all purchased from BD
522 Bioscience, San Jose, CA, USA, unless noted otherwise): CD3 (clone SP34-2, V450), CD4
523 (clone L200, APC), CD8 (clone RPA-T8, PE-CF594), CD28 (clone CD28.2, PE-Cy7), CD38
524 (clone AT-1, FITC) (Stemcell), CD45 (clone D058-1283, PerCP), CD69 (clone FN50, APC-H7),
525 CD95 (clone DX2, FITC), HLA-DR (clone L243, PE-Cy7), Ki-67 (clone P56, PE). For
526 intracellular staining, cells were fixed and permeabilized with 1X BD Fix/Perm, before being
527 stained for Ki-67. Flow cytometry acquisitions were performed on an LSRFortessa flow
528 cytometer (BD Biosciences), and flow data were analyzed using FlowJo® v10.8.0 (TreeStar,
529 Ashland, OR, USA).
530
531 **Spike-Specific Intracellular Staining**
532 Antigen-specific T-cell responses in the PBMC's of RMs immunized as described above
533 were analyzed after immunization by flow cytometry, adhering to the recently published
534 guidelines.[21,82] PBMCs collected prior to immunization and on Day 42 post prime immunization
535 were stimulated with PepTivator SARS-CoV-2-S1 (a pool of S1 MHC class I– and MHC class
536 II– restricted peptides) overnight in the presence of protein transport inhibitors (Golgi Stop) for
537 the last 4 hours. Unstimulated cells were used as negative controls. Phorbol myristate acetate
538 (PMA) and ionomycin stimulated cells served as positive controls. Cell were washed with FACS
539 buffer (PBS, 2 % FCS), incubated with Fc Block (BD Biosciences, 553142) for 5 min at 4°C,
540 and stained with surface marker antibody (Ab) stain for 20 min at 4°C. Surface Abs were used as
541 follows: CD3-V450 (SP34-2, V450, BD Biosciences), CD4-APC (L200, APC, BD Biosciences),

and CD8ab-PE-CF594 (RPA-T8, PE-CF594, BD Biosciences). For dead cell exclusion, cells were stained with Zombie NIR Fixable Viability dye (BioLegend) for 10 min at 4°C and washed in FACS buffer. Intracellular cytokine staining (ICS) was performed on surface Ab-stained cells by first fixing and permeabilizing cells using the FoxP3 Transcription Factor Staining Buffer kit (eBioscience, 00-5523-00) following manufacturer's instructions. Intracellular staining with IFNγ-FITC (4S.B3, FITC, BD Biosciences), IL2-PE (MQ1-17H12, PE, BD Biosciences), and TNFa-AF700 (Mab11, AF700, BD Biosciences). Samples were run on an Aurora (Cytek) flow cytometer and flow data were analyzed using FlowJo® v10.8.0 (TreeStar, Ashland, OR, USA).

Statistical Analysis

Statistical analyses were performed using GraphPad Prism v9 (San Diego, CA). Significant differences are indicated by * $p < 0.05$. Comparisons with non-significant differences are not indicated.

Acknowledgements

This work was supported by the National Institutes of Health/National Institute of Diabetes and Digestive and Kidney Diseases/National Institute of Allergy and Infectious Diseases grants R01 DK119936 (CA), R01 DK131476 (CA), R01 AI119346 (CA), R01 DK130481 (IP), R01 DK113919 (IP/CA). AJK was supported in part by the NIH Pitt AIDS Research Training (PART) grant (AI065380) and by the NIAID T32 grant Immunology of Infectious Diseases (IID) (AI060525). AG is funded by NIH grants (UM1-AI106701, R01DK119936-S1 and U01-CA233085) and UPMC Enterprises IPA 25565. The funders had no

role in study design, data collection and analysis, decision to publish, or preparation of the manuscript.

Disclosure

The authors declare that they have competing interests in relation to the research presented in this manuscript. AG, EK, and MSK are co-founders of GAPHAS PHARMACEUTICAL INC., a private startup company that may potentially benefit from the findings of this research. AG, EK, and MSK have equity in GAPHAS PHARMACEUTICAL INC. However, the authors have taken measures to ensure that the research is conducted objectively and that the data and conclusions presented in this manuscript are not influenced by their competing interests. The study was designed, conducted, and analyzed independently of the company. The authors also declare that GAPHAS PHARMACEUTICAL INC. did not provide financial or material support for this research.

References

1. WHO Coronavirus (COVID-19) Dashboard. https://covid19.who.int.
2. Ada, G. Overview of vaccines and vaccination. *Mol Biotechnol* **29**, 255–72 (2005).
3. Tatar, M., Shoorekchali, J. M., Faraji, M. R. & Wilson, F. A. International COVID-19 vaccine inequality amid the pandemic: Perpetuating a global crisis? *J. Glob. Health* **11**, 03086–03086 (2021).
4. WHO – COVID19 Vaccine Tracker. https://covid19.trackvaccines.org/agency/who/.
5. Krause, P. R. *et al.* SARS-CoV-2 Variants and Vaccines. *N. Engl. J. Med.* **385**, 179–186 (2021).

6. Harvey, W. T. *et al.* SARS-CoV-2 variants, spike mutations and immune escape. *Nat Rev Microbiol* **19**, 409–424 (2021).

7. Ahmad, L. Implication of SARS-CoV-2 Immune Escape Spike Variants on Secondary and Vaccine Breakthrough Infections. *Front. Immunol.* **12**, (2021).

8. Hoffmann, M. *et al.* SARS-CoV-2 variants B.1.351 and P.1 escape from neutralizing antibodies. *Cell* **184**, 2384-2393.e12 (2021).

9. Walls, A. C. *et al.* Structure, Function, and Antigenicity of the SARS-CoV-2 Spike Glycoprotein. *Cell* **181**, 281-292.e6 (2020).

10. Yan, R. *et al.* Structural basis for the recognition of SARS-CoV-2 by full-length human ACE2. *Science* **367**, 1444–1448 (2020).

11. Huang, Y., Yang, C., Xu, X., Xu, W. & Liu, S. Structural and functional properties of SARS-CoV-2 spike protein: potential antivirus drug development for COVID-19. *Acta Pharmacol. Sin.* **41**, 1141–1149 (2020).

12. Ng, K. T., Mohd-Ismail, N. K. & Tan, Y.-J. Spike S2 Subunit: The Dark Horse in the Race for Prophylactic and Therapeutic Interventions against SARS-CoV-2. *Vaccines* **9**, 178 (2021).

13. Jiang, S., Hillyer, C. & Du, L. Neutralizing Antibodies against SARS-CoV-2 and Other Human Coronaviruses. *Trends Immunol* **41**, 355–359 (2020).

14. Garcia-Beltran, W. F. *et al.* COVID-19-neutralizing antibodies predict disease severity and survival. *Cell* **184**, 476-488.e11 (2021).

15. Khoury, D. S. *et al.* Neutralizing antibody levels are highly predictive of immune protection from symptomatic SARS-CoV-2 infection. *Nat Med* **27**, 1205–1211 (2021).

16. Earle, K. A. *et al.* Evidence for antibody as a protective correlate for COVID-19 vaccines. *Vaccine* **39**, 4423–4428 (2021).

17. Amin Addetia *et al.* Neutralizing Antibodies Correlate with Protection from SARS-CoV-2 in Humans during a Fishery Vessel Outbreak with a High Attack Rate. *J. Clin. Microbiol.* **58**, e02107-20 (2020).

18. Gao, W. *et al.* Effects of a SARS-associated coronavirus vaccine in monkeys. *Lancet* **362**, 1895–6 (2003).

19. Kim, E. *et al.* Immunogenicity of an adenoviral-based Middle East Respiratory Syndrome coronavirus vaccine in BALB/c mice. *Vaccine* **32**, 5975–5982 (2014).

20. Kim, E. *et al.* Microneedle array delivered recombinant coronavirus vaccines: Immunogenicity and rapid translational development. *EBioMedicine* **55**, 102743 (2020).

21. Khan, M. S. *et al.* Adenovirus-vectored SARS-CoV-2 vaccine expressing S1-N fusion protein. *Antib. Ther.* **5**, 177–191 (2022).

22. Khan, M. S., Kim, E., Huang, S., Kenniston, T. W. & Gambotto, A. Trivalent SARS-CoV-2 S1 Subunit Protein Vaccination Induces Broad Humoral Responses in BALB/c Mice. *Vaccines* **11**, 314 (2023).

23. Kim, E. *et al.* SARS-CoV-2 S1 Subunit Booster Vaccination Elicits Robust Humoral Immune Responses in Aged Mice. 2022.10.25.513090 Preprint at https://doi.org/10.1101/2022.10.25.513090 (2022).

24. Hansen, S. G. *et al.* Prevention of tuberculosis in rhesus macaques by a cytomegalovirus-based vaccine. *Nat. Med.* **24**, 130–143 (2018).

630 25. Shedlock, D. J., Silvestri, G. & Weiner, D. B. Monkeying around with HIV vaccines:
631 using rhesus macaques to define 'gatekeepers' for clinical trials. *Nat. Rev. Immunol.* **9**, 717–
632 728 (2009).
633 26. Vogel, A. B. *et al.* BNT162b vaccines protect rhesus macaques from SARS-CoV-2.
634 *Nature* **592**, 283–289 (2021).
635 27. Milligan, E. C. *et al.* Infant rhesus macaques immunized against SARS-CoV-2 are
636 protected against heterologous virus challenge 1 year later. *Sci. Transl. Med.* **15**, eadd6383
637 (2022).
638 28. Spinelli, M. A. *et al.* Differences in Post-mRNA Vaccination Severe Acute Respiratory
639 Syndrome Coronavirus 2 (SARS-CoV-2) Immunoglobulin G (IgG) Concentrations and
640 Surrogate Virus Neutralization Test Response by Human Immunodeficiency Virus (HIV)
641 Status and Type of Vaccine: A Matched Case-Control Observational Study. *Clin. Infect. Dis.*
642 *Off. Publ. Infect. Dis. Soc. Am.* **75**, e916–e919 (2022).
643 29. Hensley, K. S. *et al.* Immunogenicity and reactogenicity of SARS-CoV-2 vaccines in
644 people living with HIV in the Netherlands: A nationwide prospective cohort study. *PLOS*
645 *Med.* **19**, e1003979 (2022).
646 30. Chen, H. *et al.* Immunological evaluation of an inactivated SARS-CoV-2 vaccine in
647 rhesus macaques. *Mol. Ther. - Methods Clin. Dev.* **23**, 108–118 (2021).
648 31. Sui, Y. *et al.* Protection against SARS-CoV-2 infection by a mucosal vaccine in rhesus
649 macaques. *JCI Insight* **6**, (2021).
650 32. Volkmann, A. *et al.* A Capsid Virus-Like Particle-Based SARS-CoV-2 Vaccine Induces
651 High Levels of Antibodies and Protects Rhesus Macaques. *Front. Immunol.* **13**, (2022).

652 33. Yu, J. *et al.* DNA vaccine protection against SARS-CoV-2 in rhesus macaques. *Science*
653 **369**, 806–811 (2020).
654 34. Corbett, K. S. *et al.* Evaluation of the mRNA-1273 Vaccine against SARS-CoV-2 in
655 Nonhuman Primates. *N. Engl. J. Med.* **383**, 1544–1555 (2020).
656 35. Pandrea, I. *et al.* Simian immunodeficiency virus SIVagm.sab infection of Caribbean
657 African green monkeys: a new model for the study of SIV pathogenesis in natural hosts. *J.*
658 *Virol.* **80**, 4858–4867 (2006).
659 36. Pandrea, I. *et al.* Functional Cure of SIVagm Infection in Rhesus Macaques Results in
660 Complete Recovery of CD4+ T Cells and Is Reverted by CD8+ Cell Depletion. *PLOS Pathog.*
661 **7**, e1002170 (2011).
662 37. Ma, D. *et al.* Simian Immunodeficiency Virus SIVsab Infection of Rhesus Macaques as a
663 Model of Complete Immunological Suppression with Persistent Reservoirs of Replication-
664 Competent Virus: Implications for Cure Research. *J. Virol.* **89**, 6155–6160 (2015).
665 38. Viallard, J.-F. *et al.* CD8+HLA-DR+ T lymphocytes are increased in common variable
666 immunodeficiency patients with impaired memory B-cell differentiation. *Clin. Immunol.* **119**,
667 51–58 (2006).
668 39. Sandoval-Montes, C. & Santos-Argumedo, L. CD38 is expressed selectively during the
669 activation of a subset of mature T cells with reduced proliferation but improved potential to
670 produce cytokines. *J. Leukoc. Biol.* **77**, 513–521 (2005).
671 40. Quarona, V. *et al.* CD38 and CD157: a long journey from activation markers to
672 multifunctional molecules. *Cytometry B Clin. Cytom.* **84**, 207–217 (2013).

673 41. Willcox, A. C. *et al.* Macaque-human differences in SARS-CoV-2 Spike antibody
674 response elicited by vaccination or infection. *bioRxiv* 2021.12.01.470697 (2021)
675 doi:10.1101/2021.12.01.470697.
676 42. Bange, E. M. *et al.* CD8+ T cells contribute to survival in patients with COVID-19 and
677 hematologic cancer. *Nat. Med.* **27**, 1280–1289 (2021).
678 43. Rha, M.-S. & Shin, E.-C. Activation or exhaustion of CD8+ T cells in patients with
679 COVID-19. *Cell. Mol. Immunol.* **18**, 2325–2333 (2021).
680 44. Bertoletti, A., Le Bert, N. & Tan, A. T. SARS-CoV-2-specific T cells in the changing
681 landscape of the COVID-19 pandemic. *Immunity* **55**, 1764–1778 (2022).
682 45. Grifoni, A. *et al.* SARS-CoV-2 Human T cell Epitopes: adaptive immune response
683 against COVID-19. *Cell Host Microbe* (2021)
684 doi:https://doi.org/10.1016/j.chom.2021.05.010.
685 46. Guo, L. *et al.* SARS-CoV-2-specific antibody and T-cell responses 1 year after infection
686 in people recovered from COVID-19: a longitudinal cohort study. *Lancet Microbe* **3**, e348–
687 e356 (2022).
688 47. Le Bert, N. *et al.* SARS-CoV-2-specific T cell immunity in cases of COVID-19 and
689 SARS, and uninfected controls. *Nature* **584**, 457–462 (2020).
690 48. Lu, X. & Yamasaki, S. Current understanding of T cell immunity against SARS-CoV-2.
691 *Inflamm. Regen.* **42**, 51 (2022).
692 49. Moss, P. The T cell immune response against SARS-CoV-2. *Nat. Immunol.* **23**, 186–193
693 (2022).
694 50. Arunachalam, P. S. *et al.* Adjuvanting a subunit COVID-19 vaccine to induce protective
695 immunity. *Nature* **594**, 253–258 (2021).

51. T cells found in COVID-19 patients 'bode well' for long-term immunity | Science | AAAS. https://www.science.org/content/article/t-cells-found-covid-19-patients-bode-well-long-term-immunity.

52. Grimaldi Jr, G. The utility of rhesus monkey (Macaca mulatta) and other non-human primate models for preclinical testing of Leishmania candidate vaccines. *Mem. Inst. Oswaldo Cruz* **103**, 629–644 (2008).

53. Bukh, I. *et al*. Increased mucosal CD4+ T cell activation in rhesus macaques following vaccination with an adenoviral vector. *J. Virol.* **88**, 8468–8478 (2014).

54. Phares, T. W. *et al.* Rhesus macaque and mouse models for down-selecting circumsporozoite protein based malaria vaccines differ significantly in immunogenicity and functional outcomes. *Malar. J.* **16**, 115 (2017).

55. Martins, M. A. & Watkins, D. I. What Is the Predictive Value of Animal Models for Vaccine Efficacy in Humans? *Cold Spring Harb. Perspect. Biol.* **10**, a029504 (2018).

56. He, X., Hong, W., Pan, X., Lu, G. & Wei, X. SARS-CoV-2 Omicron variant: Characteristics and prevention. *MedComm* **2**, 838–845 (2021).

57. Hoffmann, M., Zhang, L. & Pöhlmann, S. Omicron: Master of immune evasion maintains robust ACE2 binding. *Signal Transduct. Target. Ther.* **7**, 1–3 (2022).

58. Juliet R. C. Pulliam *et al.* Increased risk of SARS-CoV-2 reinfection associated with emergence of Omicron in South Africa. *Science* **376**, eabn4947 (2022).

59. Kimura, I. *et al*. Virological characteristics of the SARS-CoV-2 Omicron BA.2 subvariants including BA.4 and BA.5. *Cell* **0**, (2022).

717 60. Kim, S. *et al.* Binding of human ACE2 and RBD of Omicron enhanced by unique
718 interaction patterns among SARS-CoV-2 variants of concern. *J. Comput. Chem.* **44**, 594–601
719 (2023).
720 61. Kumar, S., Karuppanan, K. & Subramaniam, G. Omicron (BA.1) and sub-variants
721 (BA.1.1, BA.2, and BA.3) of SARS-CoV-2 spike infectivity and pathogenicity: A
722 comparative sequence and structural-based computational assessment. *J. Med. Virol.* **94**,
723 4780–4791 (2022).
724 62. Triccas, J. A., Kint, J. & Wurm, F. M. Affordable SARS-CoV-2 protein vaccines for the
725 pandemic endgame. *Npj Vaccines* **7**, 1–2 (2022).
726 63. Heidary, M. *et al.* A Comprehensive Review of the Protein Subunit Vaccines Against
727 COVID-19. *Front. Microbiol.* **13**, 927306 (2022).
728 64. Vaccine Types | NIH: National Institute of Allergy and Infectious Diseases.
729 https://www.niaid.nih.gov/research/vaccine-types.
730 65. Baxter, D. Active and passive immunity, vaccine types, excipients and licensing. *Occup.*
731 *Med.* **57**, 552–556 (2007).
732 66. Forni, G. *et al.* COVID-19 vaccines: where we stand and challenges ahead. *Cell Death*
733 *Differ.* **28**, 626–639 (2021).
734 67. Rahman, F. *et al.* Cellular and humoral immune responses induced by intradermal or
735 intramuscular vaccination with the major hepatitis B surface antigen. *Hepatology* **31**, 521–7
736 (2000).
737 68. Migliore, A., Gigliucci, G., Di Marzo, R., Russo, D. & Mammucari, M. Intradermal
738 Vaccination: A Potential Tool in the Battle Against the COVID-19 Pandemic? *Risk Manag.*
739 *Healthc. Policy* **14**, 2079–2087 (2021).

740 69. Zhao, J.-H. *et al.* Enhanced immunization via dissolving microneedle array-based
741 delivery system incorporating subunit vaccine and saponin adjuvant. *Int. J. Nanomedicine* **12**,
742 4763–4772 (2017).
743 70. Goldberg, Y. *et al.* Waning Immunity after the BNT162b2 Vaccine in Israel. *N. Engl. J.*
744 *Med.* (2021) doi:10.1056/NEJMoa2114228.
745 71. Levin, E. G. *et al.* Waning Immune Humoral Response to BNT162b2 Covid-19 Vaccine
746 over 6 Months. *N. Engl. J. Med.* **385**, e84 (2021).
747 72. Peng, Q. *et al.* Waning immune responses against SARS-CoV-2 variants of concern
748 among vaccinees in Hong Kong. *eBioMedicine* **77**, (2022).
749 73. Tut, G. *et al.* Strong peak immunogenicity but rapid antibody waning following third
750 vaccine dose in older residents of care homes. *Nat. Aging* **3**, 93–104 (2023).
751 74. Modeling of waning immunity after SARS-CoV-2 vaccination and influencing factors |
752 Nature Communications. https://www.nature.com/articles/s41467-022-29225-4.
753 75. Waning Immune Humoral Response to BNT162b2 Covid-19 Vaccine over 6 Months |
754 NEJM. https://www.nejm.org/doi/full/10.1056/nejmoa2114583.
755 76. Havervall, S. *et al.* Anti-Spike Mucosal IgA Protection against SARS-CoV-2 Omicron
756 Infection. *N. Engl. J. Med.* (2022) doi:10.1056/NEJMc2209651.
757 77. Russell, M. W., Moldoveanu, Z., Ogra, P. L. & Mestecky, J. Mucosal Immunity in
758 COVID-19: A Neglected but Critical Aspect of SARS-CoV-2 Infection. *Front. Immunol.* **11**,
759 (2020).
760 78. Tang, J. *et al.* Respiratory mucosal immunity against SARS-CoV-2 after mRNA
761 vaccination. *Sci. Immunol.* **7**, eadd4853 (2022).

79. Mucosal plasma cells are required to protect the upper airway and brain from infection: Immunity. https://www.cell.com/immunity/fulltext/S1074-7613(22)00411-3.

80. Percivalle, E. *et al*. West Nile or Usutu Virus? A Three-Year Follow-Up of Humoral and Cellular Response in a Group of Asymptomatic Blood Donors. *Viruses* **12**, 157 (2020).

81. Percivalle, E. *et al*. Prevalence of SARS-CoV-2 specific neutralising antibodies in blood donors from the Lodi Red Zone in Lombardy, Italy, as at 06 April 2020. *Euro Surveill. Bull. Eur. Sur Mal. Transm. Eur. Commun. Dis. Bull.* **25**, 2001031 (2020).

82. Kim, E. *et al.* A single subcutaneous or intranasal immunization with adenovirus-based SARS-CoV-2 vaccine induces robust humoral and cellular immune responses in mice. *Eur J Immunol* **51**, 1774–1784 (2021).

FIGURE LEGENDS

Figure 1. Construction and expression of tetravalent recombinant SARS-CoV-2-S1 proteins. A. A shuttle vector carrying the codon-optimized four variants of SARS-CoV-2-S1 gene encoding N-terminal 1-661 with c-tag (EPEA) was designated as shown in the diagram. Amino acid changes in the SARS-CoV-2-S1 region of in this study is shown. ITR: inverted terminal repeat; RBD: receptor binding domain. **B.** Detection of the SARS-CoV-2-S1 proteins by western blot with the supernatant of Expi293 cells transfected with pAd/S1WU (lane2), pAd/S1Alpha (lane3), pAd/S1Beta (lane4), and pAd/S1Gamma (lane5), respectively, using rabbit anti spike of SARS-CoV Wuhan polyclonal antibody. As a negative control, mock-transfected cells were treated the same (lane 1). **C.** Purified proteins, rS1WU (lane1), rS1Alpha (lane2), rS1Beta (lane3), and rS1Gamma (lane4), isolated by c-tag affinity purification were

784 separated by SDS-PAGE and visualized by silver staining. Molecular weight marker (MW
785 marker) is indicated on the left.
786
787 **Figure 2. Antigen-specific antibody responses in rhesus macaques immunized with**
788 **tetravalent SARS-CoV-2 rS1 protein subunit vaccine. A.** Schedule of immunization and
789 blood sampling for IgG end point titration. Rhesus macaques (N=5) were immunized with 60μg
790 of tetravalent rS1 proteins of Wuhan, B.1.1.7 (Alpha), B.1.351 (Beta), and P.1 (Gamma) [15μg
791 of each antigen] mixed with AddaVax adjuvant then administered to RMs arm at week 0 and 3.
792 Syringes indicated the timing of immunization and the red drops denote times at which blood
793 was drawn. The red crosses showed euthanized times of each RM. **B.** Sera were diluted and
794 SARS-CoV-2-S1-specific antibodies were quantified by ELISA to determine the IgG endpoint
795 titer. The IgG titers at each time points were showed in each RM. The bars represent geometric
796 mean with geometric SD. **C.** Neutralizing antibodies in serum of mice prior to immunization,
797 along with week 3 and week 7 post immunization were measured using a microneutralization
798 assay (NT_{90}) with SARS-CoV-2 Wuhan, Beta, and Delta. Serum titers that resulted in 90%
799 reduction in cytopathic effect compared to the virus control were reported. Horizontal lines
800 represent geometric mean titers. Groups were compared by Kruskal-Wallis test at each time
801 point, followed by Dunn's multiple comparisons. Significant differences are indicated by *p <
802 0.05. N = 5 rhesus macaques per group for each experiment.
803 **Figure 3. Percent ACE2 binding inhibition of neutralizing antibodies against SARS-CoV-2**
804 **variants.** Antibodies in sera (diluted 1:10) capable of neutralizing the interaction between
805 SARS-CoV-2 Wuhan, Alpha (B.1.1.7), Beta (B.1.351), Gamma (P.1), Delta (B.1.617.2), Zeta
806 (P.2), Kappa (B.1.617.1), New York (B.1.516.1), India (B.1.617 and B.1.617.3) variants spike

and ACE2 were examined in all animals preimmunization and Week 7 post prime immunization with V-PLEX SARS-CoV-2 Panel 18. Groups were compared by Kruskal-Wallis test at each time point, to preimmunized sera control, followed by Dunn's multiple comparisons. Significant differences are indicated by *p < 0.05. N = 5 rhesus macaques per group for each experiment.

Figure 4. Percent ACE2 binding inhibition of neutralizing antibodies against Omicron SARS-CoV-2 variants. Antibodies in sera, diluted **A.** 1:10 and **B.** 1:100 capable of blocking the binding of SARS-CoV-2 spike including Wuhan and spikes from immune evasive variants; BA.1, BA.2, AY.4 (Delta lineage), BA.3, BA.1+R346K mutation, BA.1+L452R mutation, B.1.1.7 (Alpha), B.1.351 (Beta), and B.1.1640.2 to ACE2 were detected with a V-PLEX SARS-CoV-2 Panel 25. Groups were compared by Kruskal-Wallis test at each time point, to preimmunized sera control, followed by Dunn's multiple comparisons. Significant differences are indicated by *p < 0.05. N = 5 rhesus macaques per group for each experiment.

Figure 5. CD3, CD4, CD8, and CD20 cell counts post immunization and boost. Absolute counts of immune cells in whole blood and immunophenotyping of circulating immune cells were determined by flow cytometry. 50 µl of whole blood were added to a TruCount tube (BD Biosciences) containing an antibody mix, allowing to precisely quantify **A.** $CD45^+$ cells, **B.** $CD4^+$, **C.** $CD8^+$ T cells, and **D.** $CD20^+$ B cells in blood per µl. PMBC's from RMs were collected and analyzed on Days -1, 3, 7, 10, 14, 21, 24, 28, 31, 35, 42, 49, and 64 days post prime immunization. Individual results for each RM are depicted.

Figure 6. CD4 CD8 T cell activation post immunization and boost. Whole peripheral blood was stained with fluorescently labeled antibodies for $CD4^+$, $CD8^+$, $CD69^+$, Ki-67^+, and HLA-

DR$^+$ to investigate CD4 and CD8 activation induced by vaccination with flow cytometry. **A.** Frequencies of CD4$^+$ CD69$^+$ T cells, **B.** Frequencies of CD4$^+$ Ki-67$^+$ T cells, **C.** Frequencies of CD4$^+$ HLA-DR$^+$ CD38$^+$ T cells, **D.** Frequencies of CD8$^+$ CD69$^+$ T cells, **E.** Frequencies of CD8$^+$ Ki-67$^+$ T cells, and **F.** Frequencies of CD8$^+$ HLA-DR$^+$ CD38$^+$ T cells. PMBC's from RMs were collected and analyzed on Days -1, 3, 7, 10, 14, 21, 24, 28, 31, 35, 42, 49, and 64 days post prime immunization. Individual results for each RM are depicted.

Figure 7. T cell memory subset dynamics and induction post immunization and boost. Whole peripheral blood was stained with fluorescently labeled antibodies for CD4$^+$, CD8$^+$, CD28$^+$ and CD95$^+$. Memory subsets were defined naive, central memory (CM), and effector memory (EM) T cells using CD28$^+$ and CD95$^+$ markers. Naive T cells are CD28$^+$CD95-, CM T cells are CD28$^+$CD95$^+$, and EM T cells are CD28-CD95$^+$. **A.** Frequencies of CD4$^+$ CM T cells, **B.** Frequencies of CD4$^+$ EM T cells, **C.** Frequencies of CD4$^+$ Naive T cells, **D.** Frequencies of CD8$^+$ CM T cells, **E.** Frequencies of CD8$^+$ EM T cells, and **F.** Frequencies of CD8$^+$ Naïve T cells. PMBC's from RMs were collected and analyzed on Days -1, 3, 7, 10, 14, 21, 24, 28, 31, 35, 42, 49, and 64 days post prime immunization. Individual results for each RM are depicted.

Figure 8. **Spike-specific CD4+ T cell responses at Day 0 and Day 42 post immunization in PBMC's.** PBMC's collected prior to immunization and on Day 42 post prime immunization were stimulated with PepTivator SARS-CoV-2-S1 (a pool of S1 MHC class I– and MHC class II– restricted peptides), followed by intracellular staining (ICS) and flow cytometry to identify SARS-CoV-2 S1 specific T cells. **(A)** Frequencies of SARS□CoV□2 S1 CD4$^+$ IFN□γ^+ T cells. Individual results for each RM are depicted. **(B)** Frequencies of SARS□CoV□2 S1 CD4$^+$ IL-2$^+$

T cells. Individual results for each RM are depicted. **(C)** Frequencies of SARS□CoV□2 S1 $CD4^+$ TNFα T cells. Individual results for each RM are depicted. Day 0 PBMC responses are indicated by solid circle. Day 42 PBMC responses are indicated by solid triangle.

Supplementary Figure 1. Yield pre and post C-tag purification of each recombinant proteins after transient transfection. To evaluate the expression of rS1WU, rS1Alpha, rS1Beta, and rS1Gamma recombinant proteins, ELISA plates were coated with chimeric MAb 40150-D003 (1:750, Sino Biological) overnight at 4°C. **A.** The supernatants of Expi293™ cells transfected with pAd/S1WU, pAd/S1Alpha, pAd/S1Beta, and pAd/S1Gammawas, respectively, diluted 1:40 or **B.** purified each protein by a CaptureSelect™ C-tagXL Affinity Matrix prepacked column diluted 1:1000 in PBS-T with 1% BSA and along with each purified rS1 proteins for a standard curve were incubated overnight at 4°C. After the plates were washed, chimeric MAb 40150-D001 HRP conjugated secondary antibody (1:10000, Sino Biological) was added to each well. After the development with reagent, the reaction was determined using an ELISA reader (Molecular Devices SPECTRAmax) in same as described in materials and methods.

Supplementary Figure 2. Neutralizing antibodies at week 0, 3, and 7 using a microneutralization assay (NT_{90}) were showed in each RM with SARS-CoV-2 Wuhan, Beta, and Delta variants.

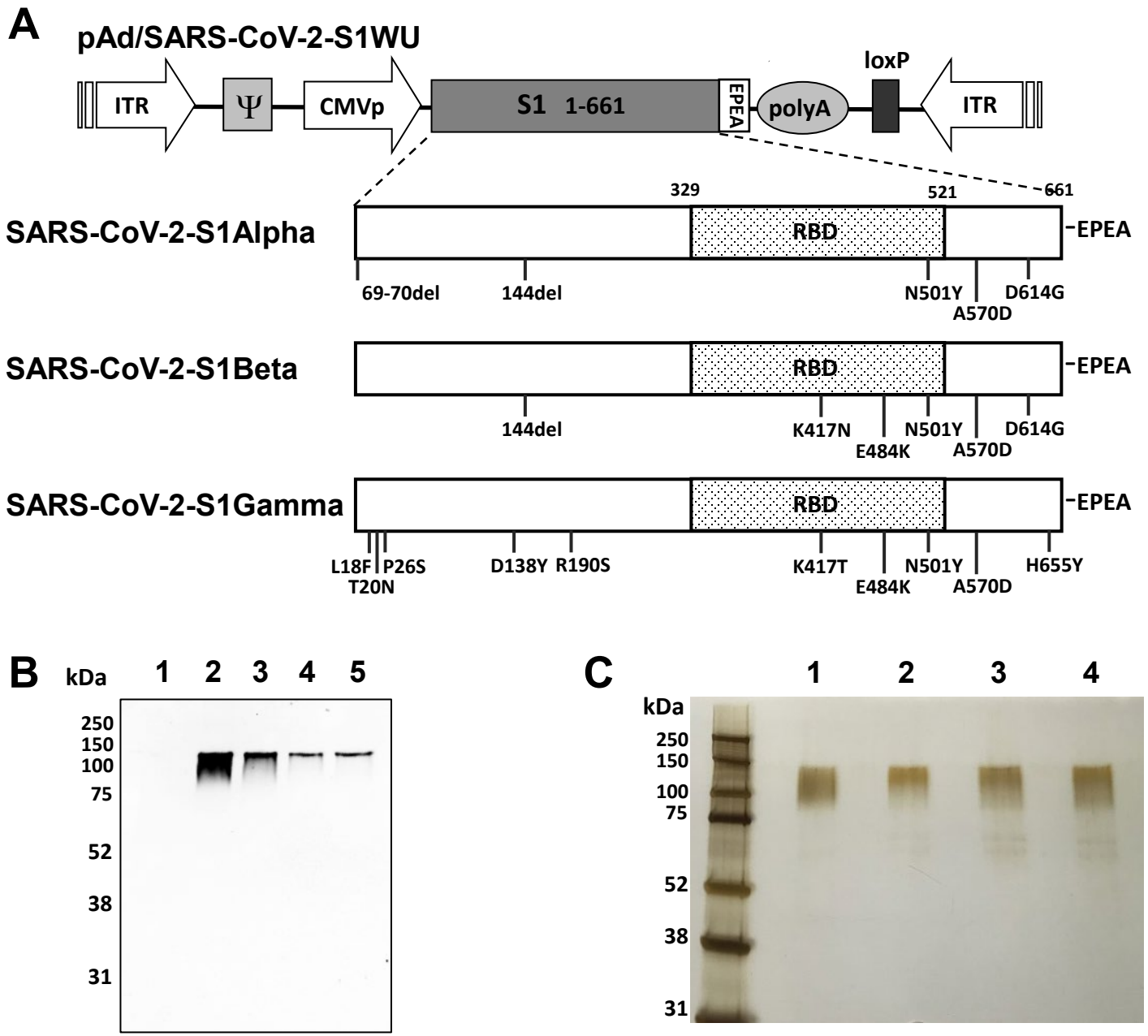
A
pAd/SARS-CoV-2-S1WU
ITR
Ψ
CMVp
S1 1-661
EPEA
polyA
loxP
ITR
329
521
661
SARS-CoV-2-S1Alpha
RBD
EPEA
69-70del
144del
N501Y
D614G
A570D
SARS-CoV-2-S1Beta
RBD
EPEA
144del
K417N
N501Y
D614G
E484K
A570D
SARS-CoV-2-S1Gamma
RBD
EPEA
L18F
T20N
P26S
D138Y
R190S
K417T
N501Y
H655Y
E484K
A570D
B
kDa
1 2 3 4 5
250
150
100
75
52
38
31
C
1 2 3 4
kDa
250
150
100
75
52
38
31

Figure 1

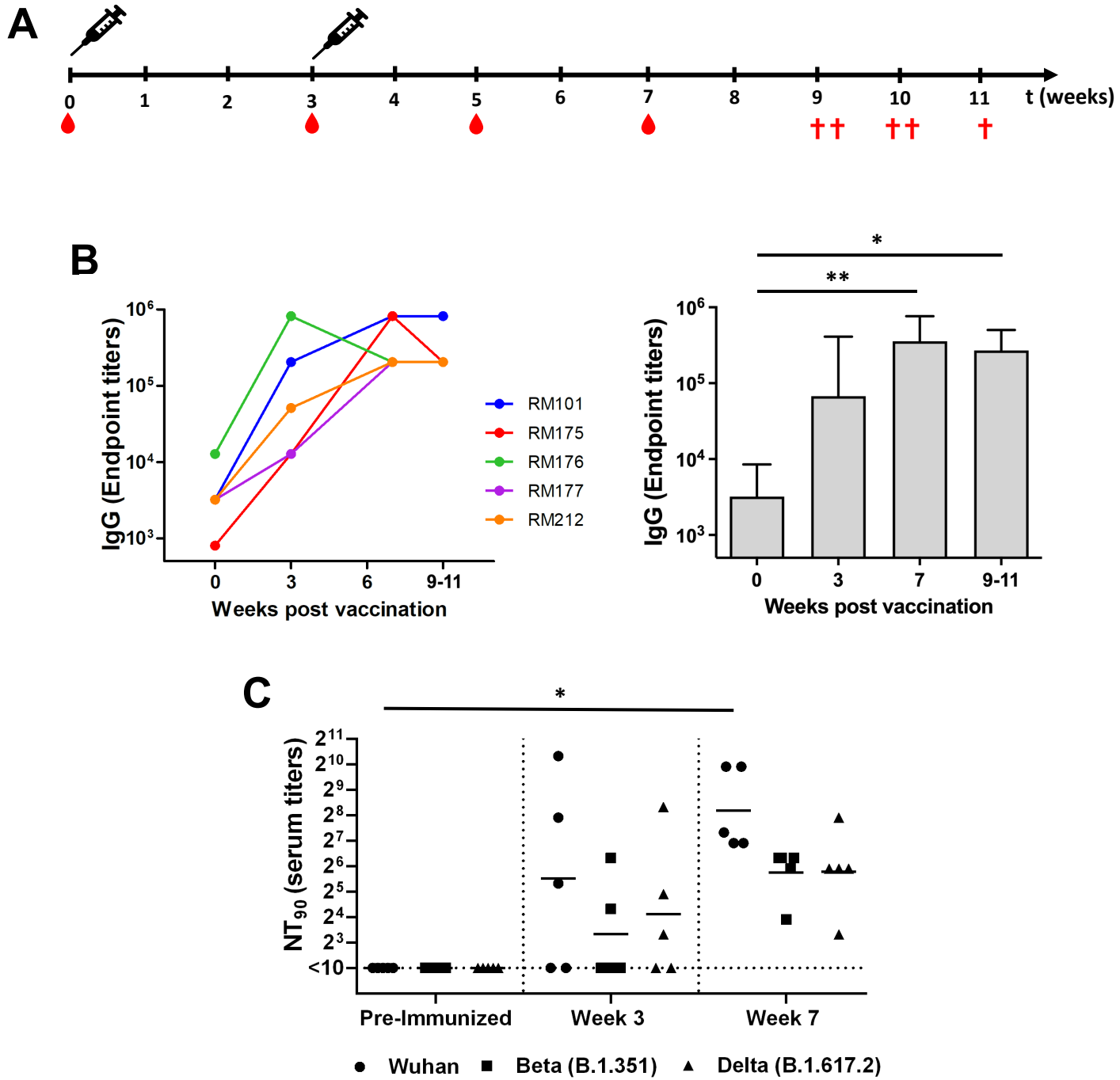
A
0
1
2
3
4
5
6
7
8
9
10
11
t (weeks)
††
††
†
B
IgG (Endpoint titers)
10^6
10^5
10^4
10^3
0
3
6
9-11
Weeks post vaccination
RM101
RM175
RM176
RM177
RM212
*
**
IgG (Endpoint titers)
0
3
7
9-11
Weeks post vaccination
C
*
NT_{90} (serum titers)
2^{11}
2^{10}
2^9
2^8
2^7
2^6
2^5
2^4
2^3
<10
Pre-Immunized
Week 3
Week 7
Wuhan
Beta (B.1.351)
Delta (B.1.617.2)

Figure 2

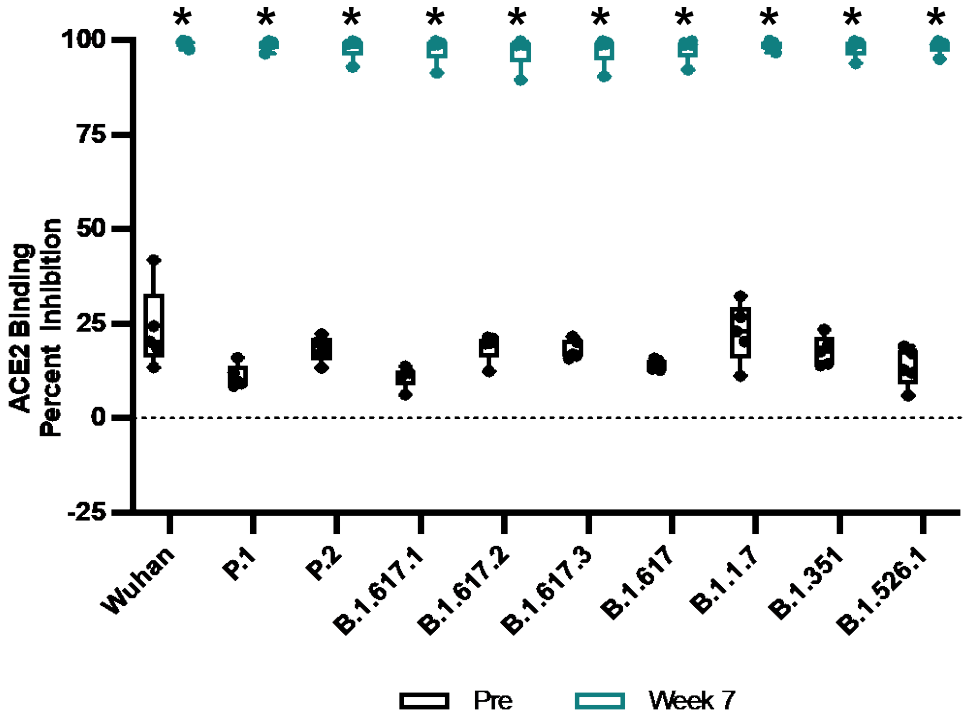
ACE2 Binding
Percent Inhibition
100
75
50
25
0
-25
*
Wuhan
P.1
P.2
B.1.617.1
B.1.617.2
B.1.617.3
B.1.617
B.1.1.7
B.1.351
B.1.526.1
Pre
Week 7

Figure 3

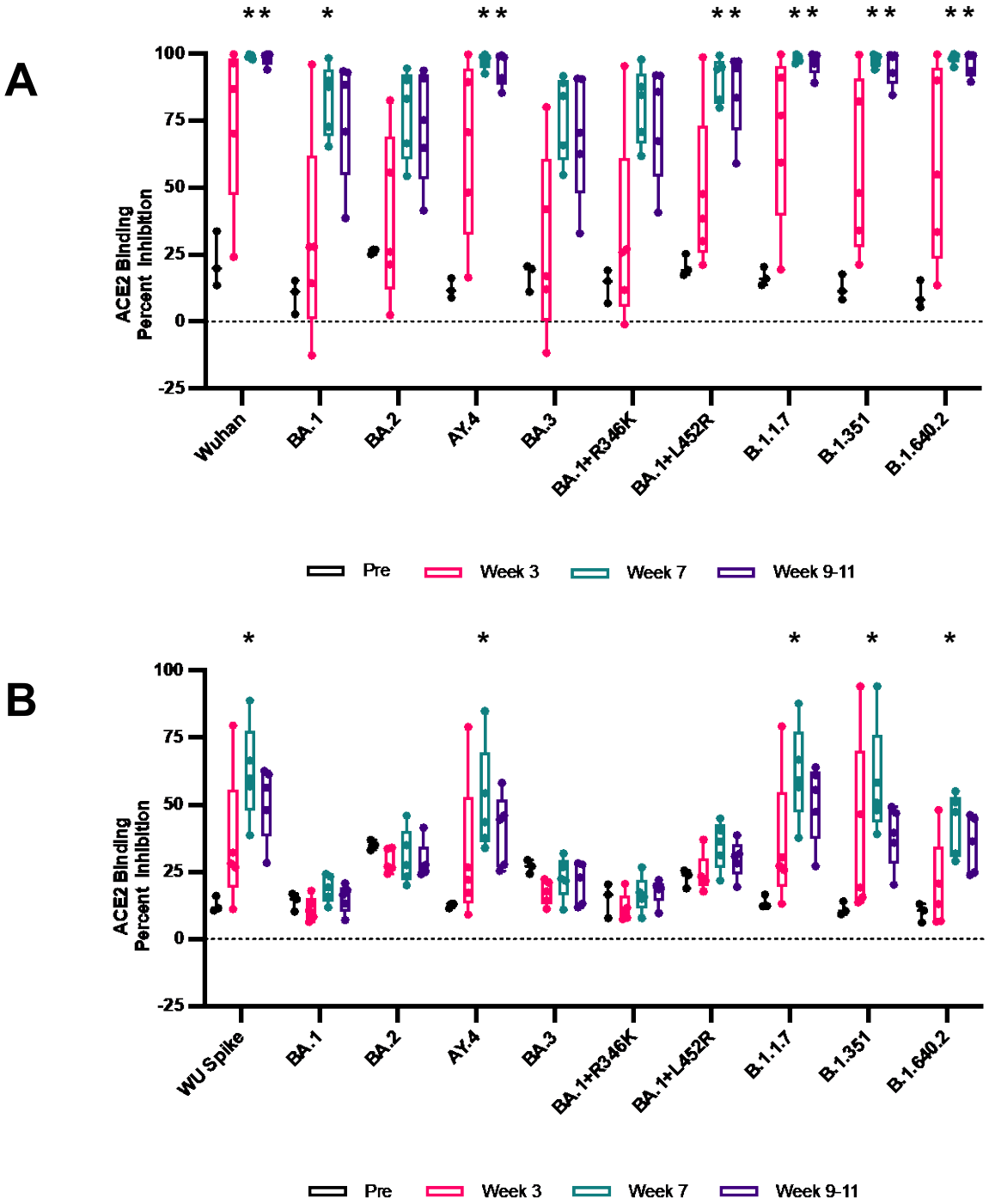
A
B
ACE2 Binding Percent Inhibition
100
75
50
25
0
-25
Wuhan
BA.1
BA.2
AY.4
BA.3
BA.1+R346K
BA.1+L452R
B.1.1.7
B.1.351
B.1.640.2
WU Spike
Pre
Week 3
Week 7
Week 9-11

Figure 4

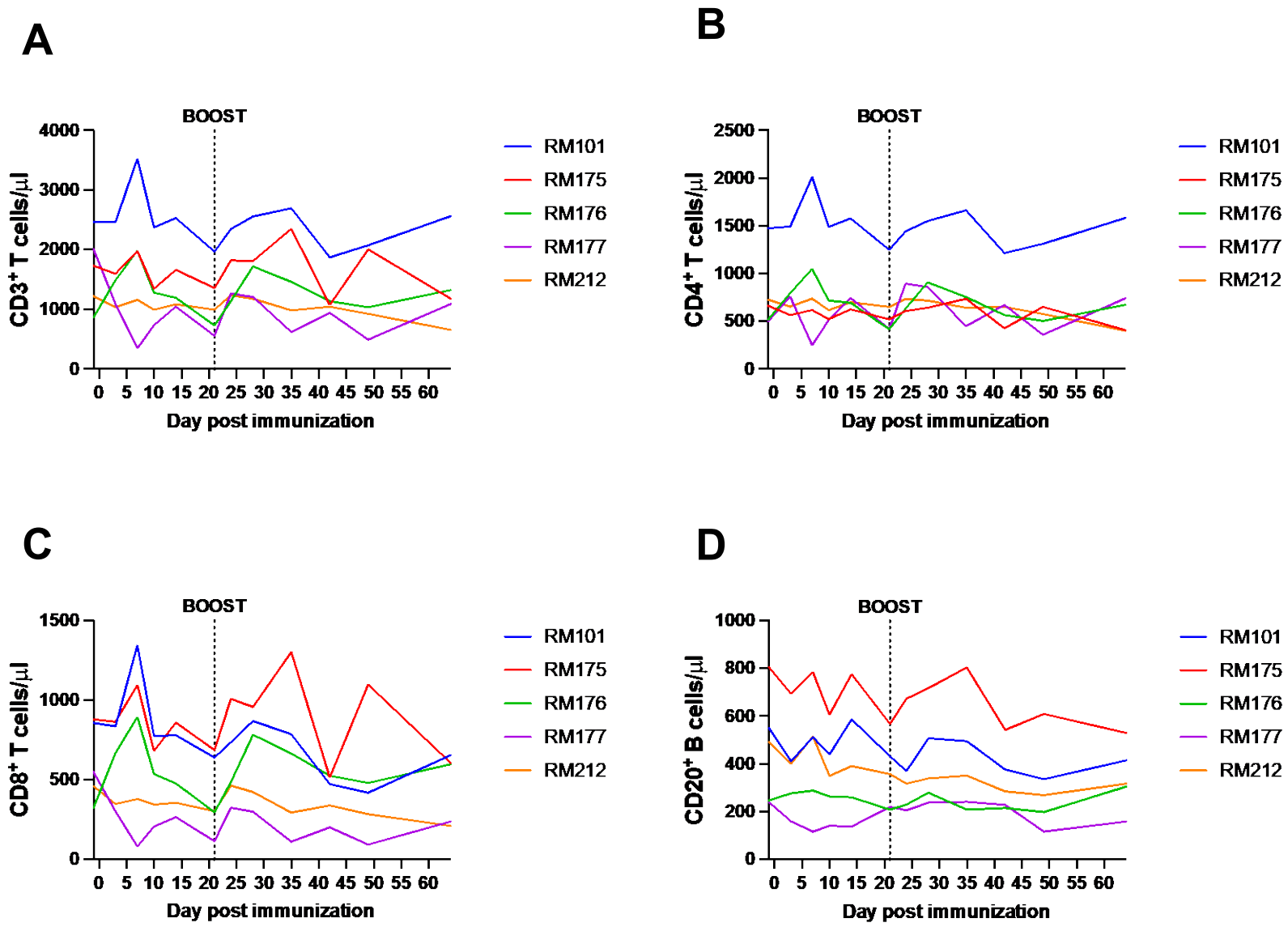
A
BOOST
CD3+ T cells/µl
4000
3000
2000
1000
0
0 5 10 15 20 25 30 35 40 45 50 55 60
Day post immunization
RM101
RM175
RM176
RM177
RM212
B
BOOST
CD4+ T cells/µl
2500
2000
1500
1000
500
0
0 5 10 15 20 25 30 35 40 45 50 55 60
Day post immunization
RM101
RM175
RM176
RM177
RM212
C
BOOST
CD8+ T cells/µl
1500
1000
500
0
0 5 10 15 20 25 30 35 40 45 50 55 60
Day post immunization
RM101
RM175
RM176
RM177
RM212
D
BOOST
CD20+ B cells/µl
1000
800
600
400
200
0
0 5 10 15 20 25 30 35 40 45 50 55 60
Day post immunization
RM101
RM175
RM176
RM177
RM212

Figure 5

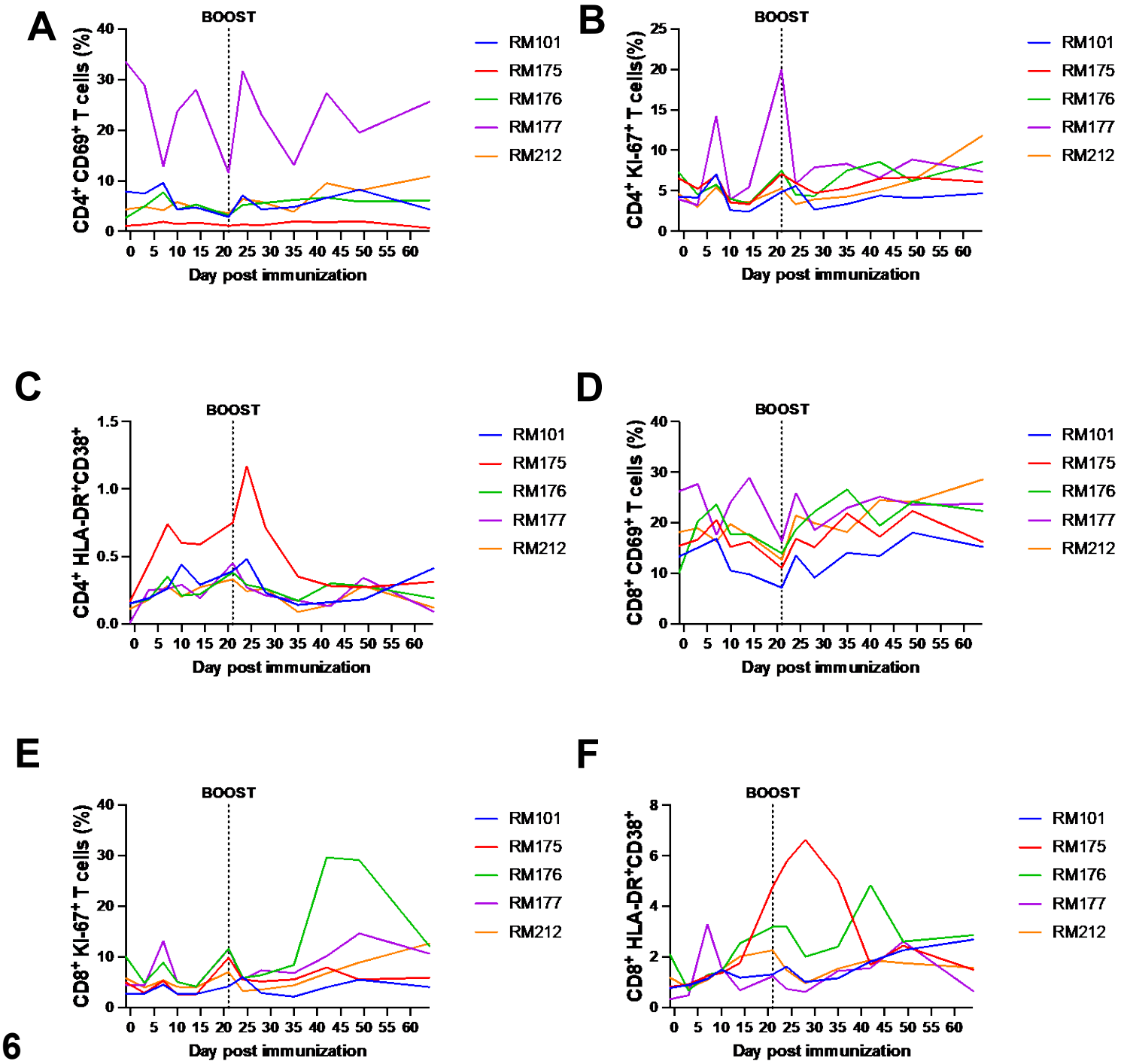
A
BOOST
CD4+ CD69+ T cells (%)
Day post immunization
RM101
RM175
RM176
RM177
RM212
B
BOOST
CD4+ KI-67+ T cells(%)
Day post immunization
RM101
RM175
RM176
RM177
RM212
C
BOOST
CD4+ HLA-DR+CD38+
Day post immunization
RM101
RM175
RM176
RM177
RM212
D
BOOST
CD8+ CD69+ T cells (%)
Day post immunization
RM101
RM175
RM176
RM177
RM212
E
BOOST
CD8+ KI-67+ T cells (%)
Day post immunization
RM101
RM175
RM176
RM177
RM212
F
BOOST
CD8+ HLA-DR+CD38+
Day post immunization
RM101
RM175
RM176
RM177
RM212

Figure 6

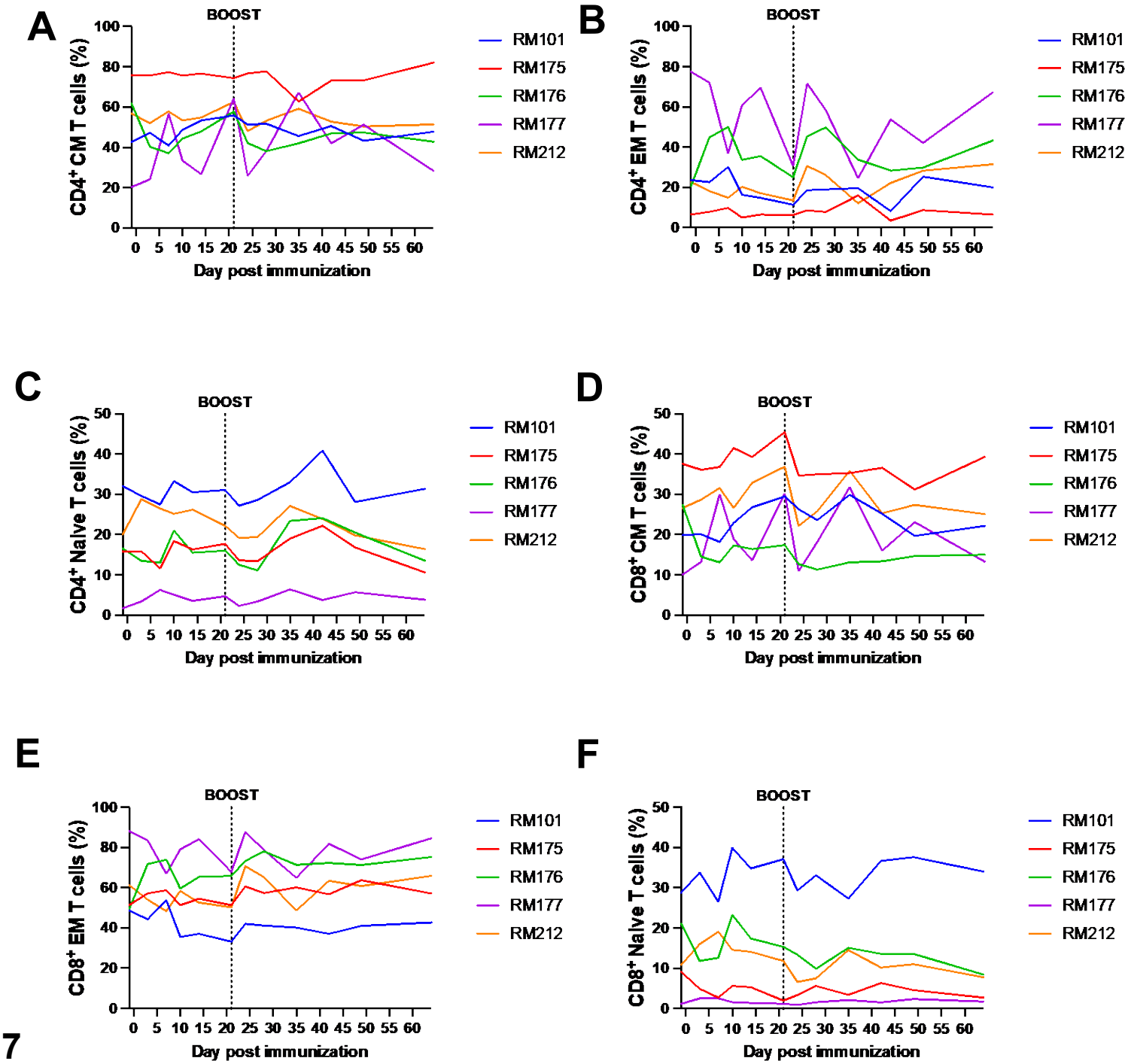
A
BOOST
CD4+ CM T cells (%)
Day post immunization
RM101
RM175
RM176
RM177
RM212
B
BOOST
CD4+ EM T cells (%)
Day post immunization
RM101
RM175
RM176
RM177
RM212
C
BOOST
CD4+ Naive T cells (%)
Day post immunization
RM101
RM175
RM176
RM177
RM212
D
BOOST
CD8+ CM T cells (%)
Day post immunization
RM101
RM175
RM176
RM177
RM212
E
BOOST
CD8+ EM T cells (%)
Day post immunization
RM101
RM175
RM176
RM177
RM212
F
BOOST
CD8+ Naive T cells (%)
Day post immunization
RM101
RM175
RM176
RM177
RM212

Figure 7

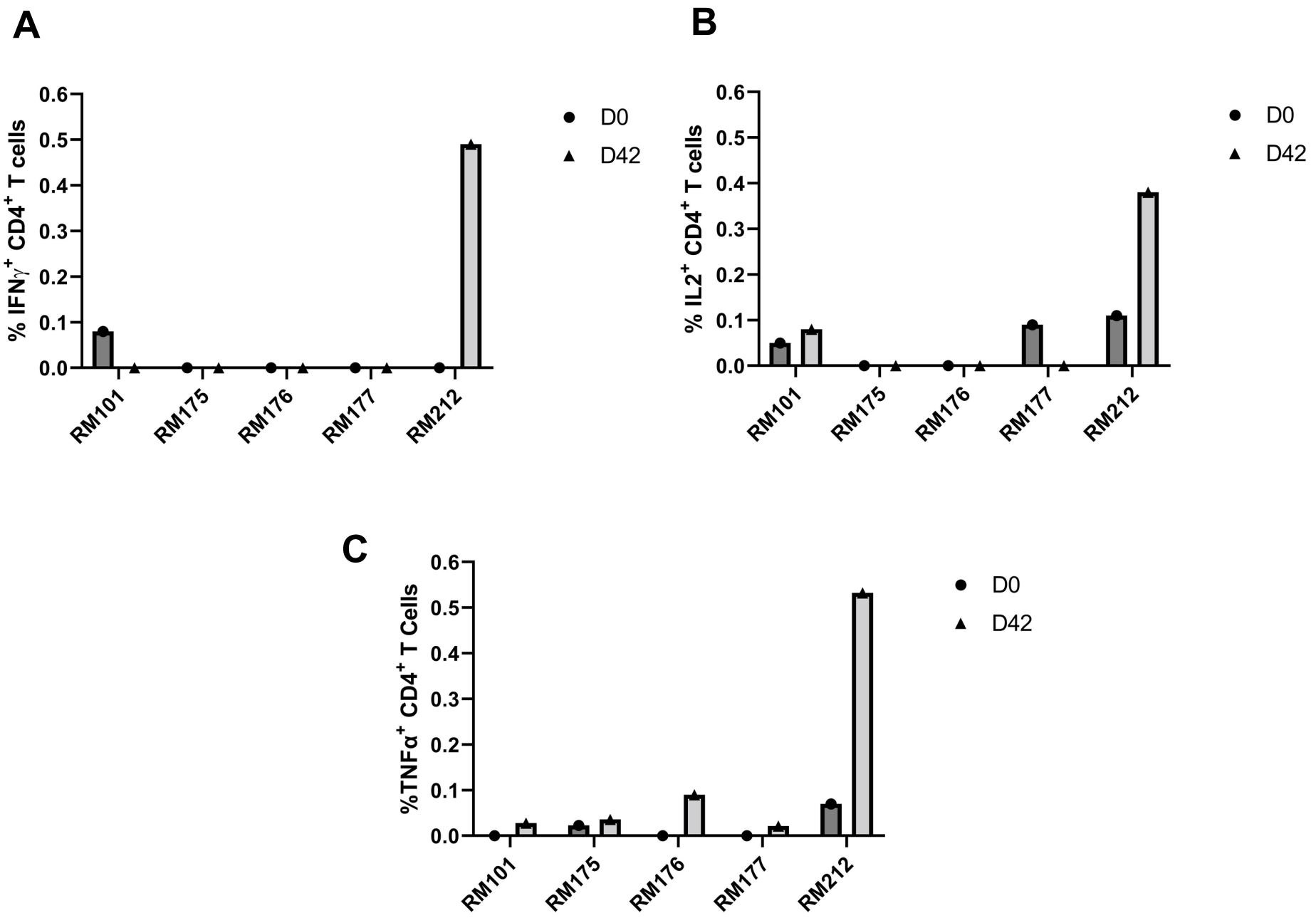
A
% IFNγ+ CD4+ T cells
0.6
0.5
0.4
0.3
0.2
0.1
0.0
RM101
RM175
RM176
RM177
RM212
D0
D42
B
% IL2+ CD4+ T cells
0.6
0.5
0.4
0.3
0.2
0.1
0.0
RM101
RM175
RM176
RM177
RM212
D0
D42
C
%TNFα+ CD4+ T Cells
0.6
0.5
0.4
0.3
0.2
0.1
0.0
RM101
RM175
RM176
RM177
RM212
D0
D42

Figure 8

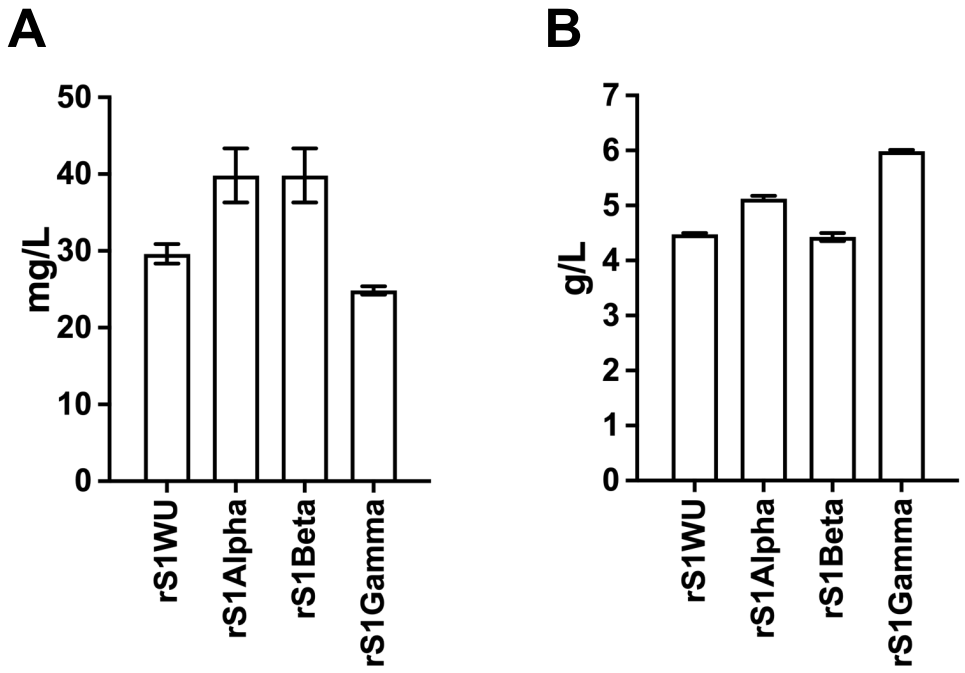

Supplementary Figure 1

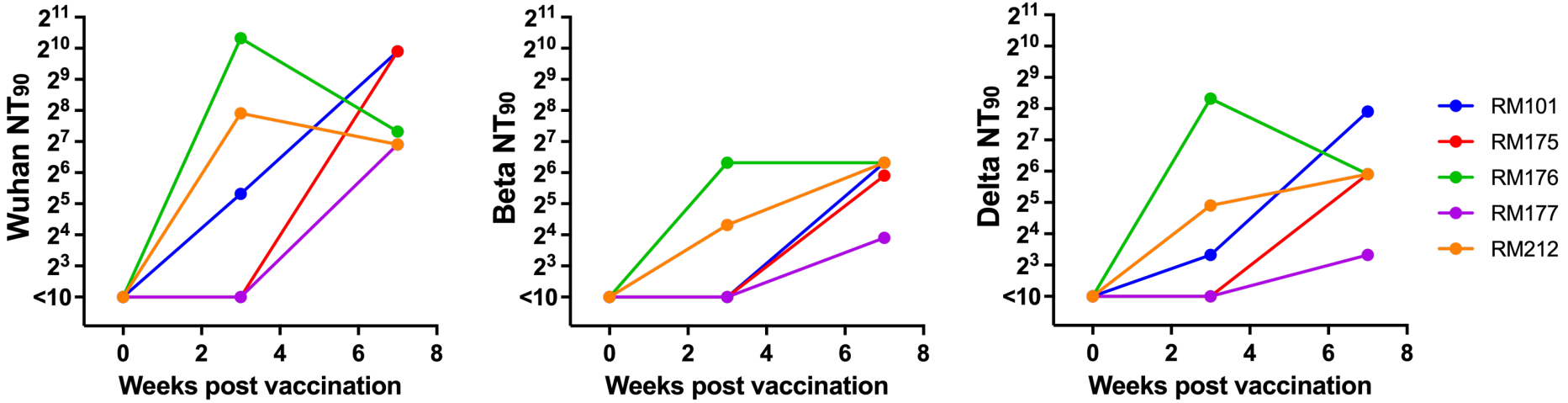

Supplementary Figure 2